Geoderma 428 (2022) 116211

Contents lists available at ScienceDirect

Geoderma

journal homepage: www.elsevier.com/locate/geoderma

Lithological controls on soil geochemistry and clay mineralogy across Spodosols in the coastal temperate rainforest of southeast Alaska

Diogo Spinola [a,b,*], Raquel Portes [c], Jennifer Fedenko [d], Rebecca Lybrand [e], Ashlee Dere [f], Frances Biles [b], Thomas Trainor [a], Mark E. Bowden [g], David D'Amore [b]

[a] Department of Chemistry and Biochemistry, University of Alaska Fairbanks, Fairbanks, AK 99775-6160, USA
[b] Forest Service, U.S. Department of Agriculture, Pacific Northwest Research Station, 11175 Auke Lake Way, Juneau, AK 99801, USA
[c] Department of Earth and Climate Sciences, Bates College, 44 Campus Ave, Carnegie Science Hall, Lewiston, ME 04240, USA
[d] Department of Crop and Soil Science, Oregon State University, Corvallis, OR 97331, USA
[e] Department of Land, Air & Water Resources, University of California, Davis, One Shields Avenue, Davis, CA 95616, USA
[f] Department of Geography and Geology, University of Nebraska, Omaha, NE, 6001 Dodge Street, 68182, USA
[g] Pacific Northwest National Laboratory, 902 Batelle Blvd, Richland, WA 99354, USA

ARTICLE INFO

Handling Editor: Alberto Agnelli

Keywords:
Lithosequence
Podzolization
Spodosols
Chemical weathering
Mineral transformation
Coastal temperate rainforest

ABSTRACT

The interaction of similar soil forming factors with different parent materials determines soil chemical weathering, influencing soil processes and properties. In the coastal temperate rainforests of southeast Alaska, Spodosols is the dominant soil order in well-drained parent materials regardless of the lithology. Yet, the role of lithology on chemical weathering, base cation depletion, and mineral transformation during pedogenesis remains elusive. Here, we established a lithosequence comprised of soils derived from tonalite, phyllite, slate, and metavolcanic rocks to test the hypothesis that despite the soils in southeast Alaska presenting similar taxonomy and morphology, the influence of lithology in chemical weathering intensity and mineralogy can be detected. We evaluated physicochemical properties, clay mineralogy, Fe-Al oxides, chemical weathering, and elemental mass balance on eleven Spodosols sampled along the lithosequence. We also propose a new weathering index, the Weathering Index for Spodosols (WISP), suitable to evaluate the weathering degree of soils with Al mobility and base-rich parent materials. This index fills a gap in traditional weathering indices that uses Al as an immobile element and/or does not evaluate the leaching of main base cations. We found the pedons across the lithosequence expressed similar physicochemical properties, with predominantly thick profiles, presenting andic properties, relatively thick spodic horizons, and thin E horizons. Podzolization imposed similar mineral transformation trends, mainly dissolution of chlorite, mica alteration to interstratified mica-vermiculite, and formation of smectite in E horizons. Kaolinite was detected in the soils from all lithologies, but only in trace amounts in phyllite soils. Fe oxides depth distribution was similar but with a higher concentration in the slate (44.5 ± 4.2 g/kg), followed by metavolcanic (31.6 ± 4.0 g/kg), phyllite (27.9 ± 3.8 g/kg), and tonalite soils (19.9 ± 5.7 g/kg) and predominantly as organometallic complexes (extracted by Na-pyrophosphate). The stronger weathering of chlorite and mica in the E horizons was reflected in larger losses of Mg and K, while Ca and Na were more depleted in the spodic horizons, suggesting plagioclase weathering. Slate soils were the most depleted in base cations, followed by phyllite, tonalite, and metavolcanic soils. The more depleted status of slate soils was supported by the higher WISP values (WISP = 62), followed by phyllite (WISP = 55), tonalite (WISP = 53), and metavolcanic soils (WISP = 45). Our results demonstrated that lithology controlled elemental depletion intensities, Fe oxide concentrations, and partially the clay fraction mineralogy in addition to podzolization acting as a dominant pedogenic process across all sites. These findings advance our understanding of the role of lithology on soil mineralogy/geochemistry that impacts critical soil functions, such as the soil carbon cycle, elemental fluxes, organo-mineral interactions, and solid-solution reactions.

* Corresponding author.
E-mail address: dspinola@alaska.edu (D. Spinola).

https://doi.org/10.1016/j.geoderma.2022.116211
Received 28 April 2022; Received in revised form 27 September 2022; Accepted 1 October 2022
Available online 26 October 2022

1. Introduction

Parent material is a soil forming factor that exerts a strong influence on soil genesis and the long-term trajectory of several properties, such as soil geochemistry, clay mineralogy, Fe/Al oxides, texture, and related physico-chemical properties (Birkeland, 1984; Hunt et al., 2021; Yaalon, 1971). In turn, soil properties greatly influence soil ecosystem services, such as soil carbon cycling (Kleber et al., 2021; Kögel-Knabner et al., 2008; Kögel-Knabner and Amelung, 2021; Von Lützow et al., 2008), element fluxes (Chadwick et al., 1990; Egli and Fitze, 2000), and solid-solution interface reactions (Stumm and Morgan, 1996; Velde and Meunier, 2008). Therefore, understanding how parent material affects soil properties is a key consideration for evaluating the role soils play in nutrient and organic carbon cycling under changing environmental conditions.

The physicochemical composition of parent materials can limit or enhance the development of soil orders. Coarse-textured, quartz-rich, and acidic parent materials under cool, humid climates and coniferous vegetation are the optimal conditions for Spodosols genesis (Lundström et al., 2000; McKeague et al., 1983; van Breemen and Buurman, 2003). Conversely, Fe and nutrient-rich, fine-textured parent materials might constrain Spodosol development (Duchaufour and Souchier, 1978; Musielok et al., 2021; Sanborn et al., 2011). Consequently, Spodosols are moderately to highly weathered soils, particularly in the E horizons due to stronger base cations and Fe depletion (Courchesne et al., 1996; Egli et al., 2004, 2003; Kindler et al., 2011; Lundström, 1993; Skiba, 2007).

The formation of pedogenic Fe-Al oxides as organometallic complexes and the vertical distribution by eluviation/illuviation processes are the core of podzolization and are considered critical for organic carbon stabilization in Spodosols (Buurman and Jongmans, 2005; Kögel-Knabner and Amelung, 2021; Lützow et al., 2006; Rasmussen et al., 2018). Although research on phyllosilicate clay minerals in Spodosols has received less attention than pedogenic Fe and Al oxides, weathering trends have been reported including the progressive transformation of mica and chlorite into vermiculite, interstratified mica-vermiculite, and hydroxy-interlayered vermiculite (Bain et al., 1990; Egli et al., 2001; Kitagawa, 2005; Meunier, 2007; Righi et al., 1993; Wilson, 1999). The further transformation from mica and vermiculite to smectite within E horizons is also common due to enhanced losses of K and Fe, and the presence of kaolinite has also been reported in the spodic and E horizons (Hunt et al., 2021; Mirabella et al., 2002; Skiba, 2007, 2001).

Spodosols formed from Fe-rich and fine textured parent materials have not been thoroughly studied likely due to their limited geographic distribution. However, in the Northeast Pacific coastal temperate rainforest of North America (NPCTR), the bioclimatic conditions (i.e., per-humid and cool climate combined with dense coniferous forest), enable podzolization to take place in mafic parent materials (Alexander et al., 1994) and on limestone (Soil Survey Staff, 2022). These are parent materials that would limit podzolization in most other regions worldwide due to less favorable bioclimatic conditions (e.g., drier, less conductive vegetation for podzolization). Assessing Spodosol genesis under particular bioclimatic conditions can, therefore, expand previously established thresholds for Spodosols formation (Duchaufour and Souchier, 1978; Musielok et al., 2021) and advance our understanding of podzolization processes.

In the NPCTR, the bioclimatic conditions also result in one of the fastest podzolization rates worldwide (Alexander and Burt, 1996; Burt and Alexander, 1996; Sauer et al., 2007; Singleton and Lavkulich, 1987). For example, the formation of Spodosols occurs in under 300 yrs on coarse-textured till deposits in southeast Alaska (Alexander and Burt, 1996; Chandler, 1943; Ugolini, 1966) and <400 yrs on sandy beach deposits in coastal British Columbia (Singleton and Lavkulich, 1987). These rates are considerably faster than in other temperate regions, where the formation of Spodosols in acidic parent materials has been shown to take from 3 ky to 11 ky in the Swiss Alps (Egli et al., 2001), and 1 ky-6 ky in Scandinavia (Mokma et al., 2004; Sauer et al., 2008). In North America, it can take between 4 ky–10 ky in Michigan (Barrett and Schaetzl, 1992), up to 15 ky in the Central Rocky Mountains (Portes et al., 2018), and between 1 ky–4,5 ky in Ontario, Canada (Protz et al., 1988, 1984).

As a result of the bioclimatic conditions and fast soil-forming rates, the soil distribution in southeast Alaska follows a predictable pattern, where Spodosols dominate stable upland landscape positions on well-drained parent materials regardless of the lithology, followed by Spodosols with aquic moisture regimes on lower backslope, and Histosols, which forms on poorly drained footslope and toeslope positions (D'Amore et al., 2012, 2015). Despite the relative heterogeneous lithologies on well-drained uplands, only a few studies have investigated the influence of different rock types on Spodosol properties in the region (Alexander et al., 1994; Heilman and Gass, 1974). These studies found that strong podzolization process overprinted the influence of lithology in terms of soil taxonomy, morphology, and exchangeable soil chemistry (e.g., pH, CEC, base saturation) (Heilman and Gass, 1974) supporting the notion that Spodosol development in the NPCTR is not limited by the rock type. However, an assessment of Spodosols geochemistry and mineralogy from different parent materials have not yet been done to date.

Obtaining a better understanding of the role of lithology on the geochemical and mineralogical properties of Spodosols would improve our ability to predict and spatially model soil properties (e.g., soil organic carbon, nutrient availability, texture) at a regional scale as a function of lithology in addition to other landscape parameters (e.g., topography). Moreover, research on Spodosols geochemistry and mineralogy in coastal temperate rainforests is scarce when compared to Spodosols in more continental temperate climates, such as in North-Central Europe and North America (Sauer et al., 2007). The coastal temperate rainforests are among the richest ecosystems in terms of soil organic carbon stocks (Kramer and Chadwick, 2018; McNicol et al., 2019). Therefore, further investigation is required on mineral weathering and secondary mineral formation, which could impact soil organic carbon dynamics and nutrient cycling given the important role that mineral weathering play in those soil ecosystem services.

The objectives of this study are to 1) investigate the genesis of Spodosols across a lithosequence in the coastal temperate rainforest of southeast Alaska; 2) compare the degree of soil weathering and elemental losses/gains, and; 3) evaluate the role of lithology and podzolization on silicate weathering to clay minerals and Fe/Al oxides. We hypothesized that despite Spodosols in the temperate rainforest of southeast Alaska presenting similar taxonomy and morphology, the influence of lithology in soil geochemistry and mineralogy can be detected. More specifically, we predicted that vertical trends in chemical weathering and mineralogical transformation are dictated by podzolization, in line with field observations and previous publications (Alexander et al., 1993; Heilman and Gass, 1974) but the intensity of elemental depletion and clay mineral concentrations (including Fe-Al oxides) vary with rock type. Our findings contribute to a better understanding of the influence of lithology on elemental leaching and secondary mineral formation in a temperate rainforest environment with potential implications for soil ecosystem services.

2. Materials and methods

2.1. Study site

The study area is within the Northeast Pacific coastal temperate rainforest of North America, which represents the largest coastal temperate rainforest in the world, extending from California to southeast Alaska (Wolf et al., 1995). We focused our work on a sequence of soils selected near Juneau, Alaska (Fig. 1) where the climate is characterized by abundant precipitation (mean annual precipitation of 1400 mm and 2400 mm as snowfall) without a dry season and a mean average

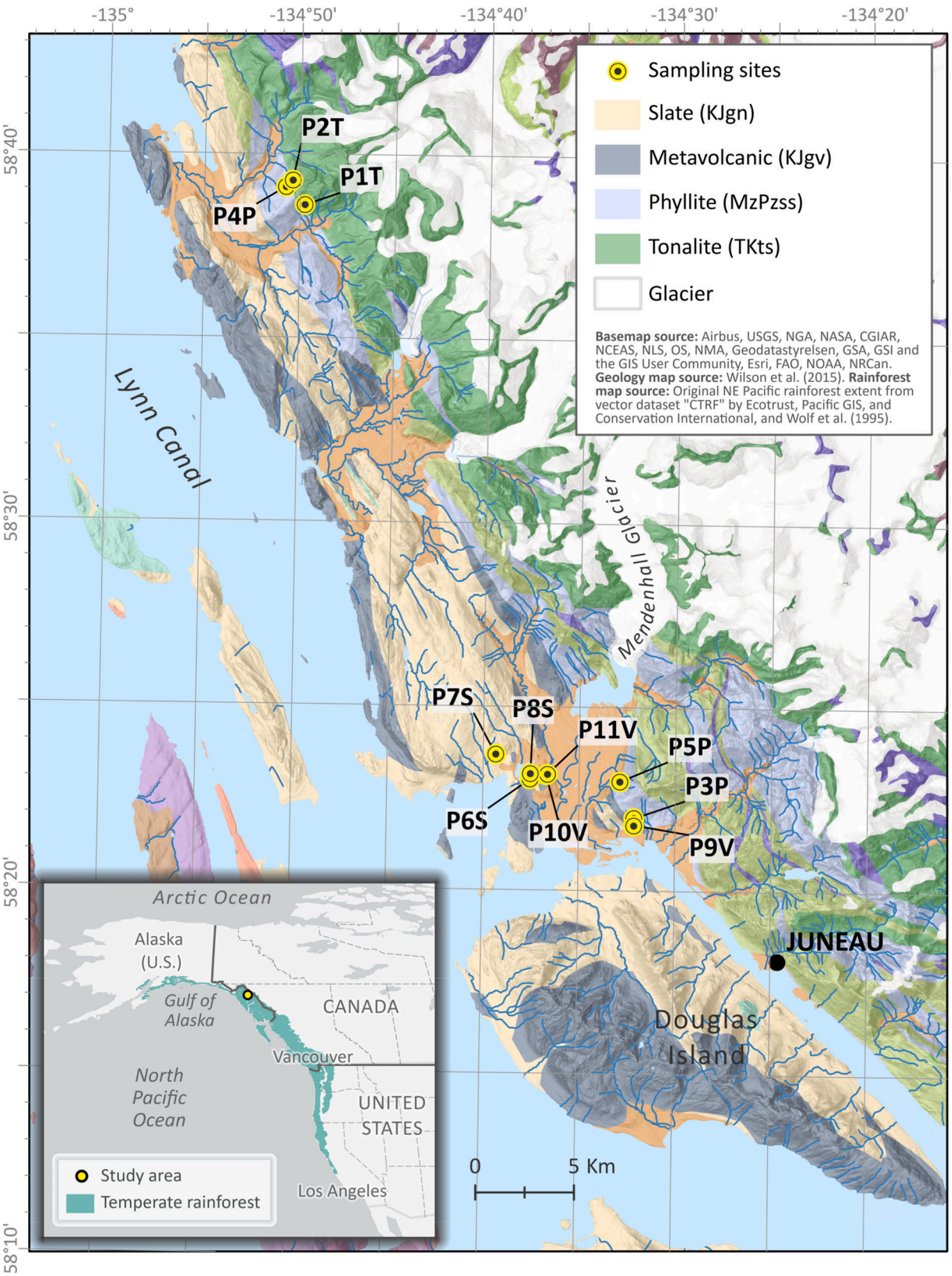

Fig. 1. Location of the study area in Juneau, SE Alaska. It includes the extent of the Coastal Temperate Rainforest of North America, and the predominant geology. Yellow circles represent the sampling sites.

temperature of 4.7 °C at sea level (Alaback and Pojar, 1997; National Climatic Data Center, 2020). The soils of the region have a cryic temperature regime and udic-to-perudic soil moisture regimes (Ping et al., 2017).

The major tree species at the study sites are western hemlock (*Tsuga heterophylla*), mountain hemlock (*Tsuga mertensiana*), Sitka Spruce (*Picea sitchensis*), and Sitka alder (*Alnus rubra*) (Heusser, 1960). The forest understory is dominated by blueberry (*Vaccinium ovalifolium*), deviĺs club (*Oploplanox horridus*), and the forest floor is generally covered by a carpet of moss, comprised mostly of Rhytidiadelphus and *Hylocomium ssp*. (Heilman and Gass, 1974).

The landscape of southeast Alaska was formed through the accretion of terranes with varying lithologies associated with the subduction of the Pacific plate under the North American continent. The terranes consist of several lithologies including sedimentary, volcanic, metamorphic, and intrusive bedrocks ranging in age from Triassic to Paleocene (Gehrels and Berg, 1992; Miller, 1975). Glacial periods formed landscapes with wide U-shaped valleys, deep fjords, and jagged and rounded mountain summits (Brock et al., 1996). Landforms include mountains and hillslopes covered by unconsolidated Quaternary deposits (colluvial, glacial, glaciomarine, alluvial, deltaic, and beach deposits) (FS-R10-TNF, 2016). During the Last Glacial Maximum, most of the southeast Alaska region was covered by the Cordilleran Ice Sheet (CIS) (Carrara et al., 2007; Lesnek et al., 2018). Recent ^{10}Be surface exposure ages of the region indicate that the earliest retreat of the CIS occurred from ~11 to ~15 ka (Lesnek et al., 2020).

The soils were sampled on colluvial deposits derived from the rocks belonging to the Taku terrane, Gravina belt, and the Coast Mountain batholith (Fig. 1). The lithologies of the colluvial deposits include tonalite (Coast Mountain batholith, in Héen Latinee Experimental Forest), phyllite (Taku terrane), slate, and metavolcanic, both belonging to the Gravina belt (Gehrels and Berg, 1994). The lithological composition of the colluvial deposits was confirmed after field inspection of the dominant rock fragments in the profile and by petrographic descriptions (data not shown). The lithologies are distributed parallel to each other on the landscape along a SE-NW longitudinal setting due to the history of terrane accretion. The landscape arrangement provides an ideal spatial context to establish a lithosequence study, where climate, landform, vegetation, and altitude, are all similar and only lithology varies across sites.

The dominant mineralogical composition of phyllite and slate are similarly composed of quartz, chlorite, albite (Na-plagioclase), muscovite, and biotite (section 3.2 – Table 3, Supplementary Fig. 1). Phyllite has a larger grain size and marked preferential orientation of mica, which provides a characteristic reflective sheen not seen on the slate. Tonalite is composed of anorthite (Ca-plagioclase), quartz, amphibole (hornblende), albite, biotite, and muscovite (section 3.2 – Table 3, Supplementary Fig. 1). The metavolcanic lithology has a basaltic composition (McClelland et al., 1992), Supplementary Fig. 2) with a predominance of amphibole (actinolite), albite, chlorite, muscovite, epidote, and pyroxene (section 3.2 – Table 3, Supplementary Fig. 1).

2.2. Soil sampling

Eleven pedons were sampled by morphological horizons (Table 1) described following the USDA – NRCS Field Book (Schoeneberger et al., 2012) and classified using Keys to Soil Taxonomy (Soil Survey Staff, 2014a). Pedons were excavated manually with a shovel to a depth of ~1 m or to the refusal of parent material contact where it was physically prohibitive to dig further.

Samples for bulk density analysis of mineral horizons were collected using a soil volumetric core (138.5 cm^3) with two replicates, and 5 cm-sized cubes (125 cm^3) were sampled for organic horizons. Rock fragments were estimated visually in the field and confirmed in the lab after estimating the rock fragments in bulk density rings. For microprobe analysis (Section 2.6), undisturbed soil samples were collected using PVC cases and impregnated under vacuum with epoxy resin at the Department of Geology, National Autonomous University of Mexico. The impregnated blocks were sliced into 9 × 6 cm, 30 μm thick, thin sections at the National Petrographic Service Inc. (Texas, USA).

Pedons were sampled on colluvial deposits on backslope positions, where the percent slope ranged from 37 to 60 % and between 90 and 300 m above sea level (m.a.s.l). Three soils were sampled in the Héen Latinee Experimental Forest, north of Juneau, at a slightly higher elevation, between 610 and 630 m.a.s.l. However, there were no significant differences in climate, vegetation, and slope position among the different sites. Six pedons were south-facing and five were north-facing. The suffixes T, P, S, and V were designated after each pedon number to refer to the lithology: T = tonalite, P = phyllite, S = slate, and V = metavolcanic.

2.3. Laboratory analyses

Bulk soil samples were oven-dried at 50 °C, sieved to < 2 mm, and then subsampled for subsequent analyses (Fig. 2). Soil pH was determined using a glass electrode in a 1:1 soil:water solution for mineral horizons and 1:4 soil:water for organic horizons. Particle size distribution was determined by the sieving and pipette method (Soil Survey Staff, 2014b). The bulk density of the organic horizons was determined after oven-drying the samples to a constant weight at 110 °C and dividing the final mass by 125 cm^3. The bulk density of the mineral horizons was calculated from the oven-dried mass of soil after sieving out rock fragments and dividing by the sample collection volume (138.5 cm^3). Soil organic carbon (SOC) content was determined by dry combustion at 1,150 °C using an *Elementar Vario MACRO cube*.

The uniformity of the parent material was investigated along a depth profile using the percentage of rock fragments and the Uniformity Value (UV) Index (Cremeens and Mokma, 1986; Portes et al., 2016; Schaetzl, 1998). The UV index compares particle size fractions from upper and lower horizons (Eq. (1)).

Table 1
General characteristics of the sampled pedons.

Pedon	Lithology	Location (dec. degrees)		Aspect	Slope (%)	Elevation (m)
P1T	Tonalite	58.64406	−134.82907	South	75	620
P2T	Tonalite	58.65514	−134.83986	North	37	610
P3P	Phyllite	58.36695	−134.53561	South	34	218
P4P	Phyllite	58.65214	−134.84570	South	55	630
P5P	Phyllite	58.38350	−134.54805	North	65	300
P6S	Slate	58.38384	−134.62649	South	50	140
P7S	Slate	58.39552	−134.65585	South	76	180
P8S	Slate	58.38681	−134.62570	North	55	295
P9V	Metavolcanic	58.36356	−134.53561	South	31	110
P10V	Metavolcanic	58.38634	−134.61200	South	40	140
P11V	Metavolcanic	58.38660	−134.61078	North	60	90

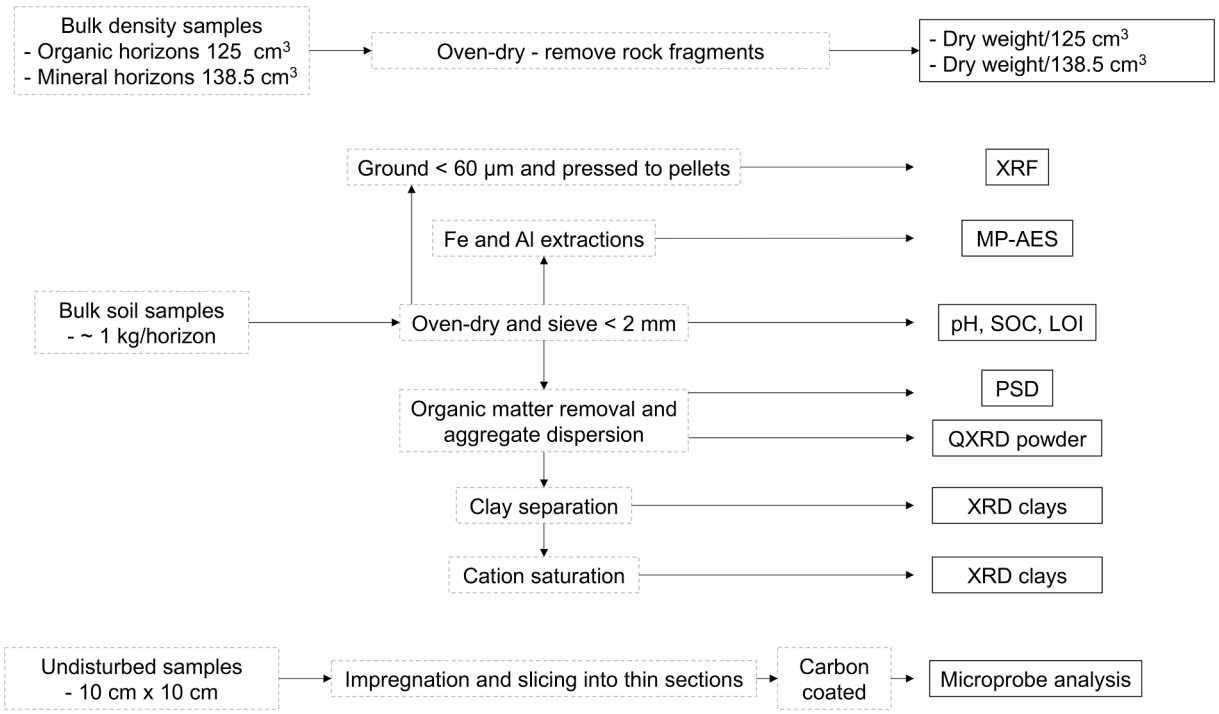

Fig. 2. A flowchart with sample preparation/treatments and analyses. Details are described in subsequent sections. Left side: sample type; middle: preparation/treatments; right side and solid lines: analyses. SOC: soil organic carbon, LOI: loss on ignition, MP-AES: microwave plasma atomic emission spectrometer, XRF: x-ray fluorescence, QXRD: quantitative x-ray diffraction, PSD: particle size distribution.

$$\text{UV index} = \frac{\frac{(\%silt+\%veryfinesand)}{(\%sand-\%veryfinesand)}intheupperhorizon}{\frac{(\%silt+\%veryfinesand)}{(\%sand-\%veryfinesand)}inthelowerhorizon} - 1 \quad (1)$$

UV values closer to zero indicate homogeneity and values exceeding ± 0.6 suggest a potential lithic discontinuity (Cremeens and Mokma, 1986). Given the colluvial origin of the deposits and the potential disturbances by tree throw, the UV Index was employed to confirm and help identify abrupt textural changes seen in the field.

2.3.1. Geochemistry and weathering index

Concentration (in wt%) of major oxides (SiO_2, TiO_2, Al_2O_3, Fe_2O_3, MgO, CaO, Na_2O, K_2O) was determined using a *PANalytical Axios (PW4400)* wavelength dispersive X-ray fluorescence (WD-XRF) spectrometer at the Advanced Instrumentation Laboratory, University of Alaska Fairbanks (AIL-UAF). Samples were analyzed and calibrated as described in (Whalen et al., 2015). Briefly, a subsample of ~10 g of the < 2 mm samples was ground to < 60 µm with a ball mill grinder. Subsequently, the material was mixed with a few drops of 5 % (wt./wt.) polyvinyl alcohol (PVA) binder and pressed under 9 metric tons of pressure into 40 mm diameter, 5 mm thick pellets. The elemental concentrations were corrected for loss of ignition (LOI), which was determined by heating ~2 g of soil at 900 °C. LOI was calculated as the percent of the dry weight that was lost on ignition. Analytical accuracy was estimated from measurements of the GRX-2 and GXR-6 standards (Jochum et al., 2005).

The weathering degree of each soil horizon was determined using the XRF data after an adaptation of the Chemical Index of Weathering (CIA) (Nesbitt and Young, 1982). The CIA is defined as.

$$CIA = [Al_2O_3/(Al_2O_3 + CaO^* + Na_2O + K_2O] \times 100 \quad (2)$$

where the formulas represent the molar concentration of each component (and CaO* refers to silicate bound Ca).

The CIA assumes that aluminum (Al) is immobile and thus the CIA will increase in value as base cations are depleted during weathering. However, in Spodosols Al is mobile due to its propensity for forming soluble organometallic complexes that migrate downward and laterally (McKeague et al., 1983; Sommer et al., 2000). Titanium (Ti) is another common immobile element in most soils. Thus, we replaced Al with Ti as the immobile element in the equation. Moreover, we included Mg to reflect the weathering of ferromagnesian minerals. Therefore, we propose the Weathering Index for Spodosols (WISP) to assess weathering in soils with high Al mobility and base-rich parent materials.

$$WISP = [TiO_2{*}10/(TiO_2{*}10 + CaO^* + Na_2O + K_2O + MgO] \times 100 \quad (3)$$

Since all soils were non-effervescent and assumed to be free of carbonates, we assume that all Ca was sourced from silicate minerals (CaO*). The observed low soil pH values are also consistent with the absence of carbonate minerals. The Ti values were multiplied by 10 to be of the same order of magnitude as the other elements. While the values of WISP are not directly comparable with the CIA, the rationale is the same: higher values indicate stronger weathering degree and lower values indicate weaker weathering degree.

Relative elemental losses and gains for each horizon were calculated using the open-system mass transport function τ_{jw} (Chadwick et al., 1990). As with the WISP, we also used Ti as the immobile element for the mass-balance calculations. The τ (Tau) values were plotted as depth-averaged for E horizons, and spodic horizons (Bh, Bhs, and Bs). The C horizons were used as the reference (p) because none of the soils were formed directly on bedrock. The tau values are calculated as.

$$\tau_{j,w} = \frac{C_{j,w} \bullet C_{i,p}}{C_{i,w} \bullet C_{j,p}} - 1 \quad (4)$$

where:τ represents the ratio of the concentration (wt %) of an element of interest (C_j) normalized to an immobile element (C_i; Ti) in the weathered product (w), to the unweathered (or weakly weathered) parent material (p) (Brimhall et al., 1991). Negative τ values indicate depletion, positive values indicate gains, and a value of zero indicates an element is stable in relation to the parent material or the net gain/loss of an element in a particular horizon is equal to zero. The tau values were

plotted by average values of E and spodic horizons. In this study, the C horizons were considered as the parent materials, and were used as the reference values and therefore were not plotted as a separate horizon.

2.3.2. X-ray diffraction (XRD)

2.3.2.1. Clay mineralogy (< 2 μm). The samples were pre-treated before X-ray diffraction (XRD) analysis by removing organic matter and by concentrating the clay fraction (< 2 μm). Briefly, organic matter was removed by mixing ~10 g of < 2 mm soil with a 6 % NaOCl "bleaching" solution (pH 9.5) at a soil-to-solution ratio of 1:50 (w/v) and shaken for 24 h at room temperature (Kaiser et al., 2002; Mikutta et al., 2005). The samples were then centrifugated at 3000 rpm for 45 min and the supernatants removed. This step was repeated five times or until the supernatants were clear. Later, the material was washed with DI to remove Na and air-dried for further processing (Kaiser et al., 2002). After the removal of organic matter, the samples were transferred to a centrifuge tube and mixed for 24 h with 5 % Na-Hexametaphosphate ($NaPO_3$) solution at a soil-to-solution ratio of 1:5 (w/v) on a soil mixer to improve aggregate dispersion (Soil Survey Staff, 2014b).

The remaining samples after the organic matter removal and aggregate dispersion treatments were further processed to concentrate the clay fraction. The sand fraction was removed by wet sieving (< 63 μm), and the remaining samples were washed with DI water and centrifuged at 3000 rpm for 30 min. The supernatant was discarded, and the remaining samples (silt + clay) were resuspended with DI water and centrifuged at 750 rpm for 8 min. The supernatant (i.e., clay fraction) was transferred to a centrifuge tube and dried out at 45 °C. Three subsamples of approximately 200 mg of the clay fraction were used for different treatments before analysis, air dried, K^+ saturation + heating to 550 °C, and Mg^{2+} saturation + glycerol solvation.

To detect potential peak damage by the organic matter removal treatment, we repeated the XRD analysis on two samples of a Bhs and a Bs horizon before and after treatments (i.e., organic matter removal and dispersion). The peak position did not change but the peak intensity improved after organic matter removal (Supplementary Fig. 3). Therefore, the following procedures were made in pre-treated samples after a slight modification of (Pansu and Jacques, 2006).

Air-dried (AD): An aliquot (200 mg) of the clay fraction was mixed with 5 mL of DI water and approximately 1 mL was pipetted onto glass slides forming a homogeneous layer after drying overnight at air temperature.

K + 550 °C: An aliquot of clay fraction was put in suspension by mixing with a 1 M KCl solution for 30 min and then exposed to an ultrasonic treatment in an ultrasonic bath for 30 s; centrifuged for 5 min at 4000 rpm and the supernatant was discarded. These steps were repeated three times but left shaking overnight in the second run. The centrifugation pellet was washed with DI, agitated, and centrifuged for 5 min at 4000 rpm. These steps were repeated three times. Approximately 1 mL was pipetted onto glass slides forming a homogeneous layer after drying overnight at air temperature. The slides were heated to 550 °C in a muffle oven before the XRD measurements.

Mg + Glycerol: An aliquot of clay fraction was put in suspension by mixing with a 1 M $MgCl_2$ solution followed by glycerol solvation. The same saturation procedure for K^+ saturation was adopted for Mg^{2+} saturation. A solution of 1:10 glycerol and water were prepared, and a few drops were pipetted onto the slides. The slides were air-dried for ~1 h before XRD measurements.

Oriented specimens on glass slides were analyzed by X-ray diffraction (XRD) using a *PANalytical X'PERT PRO* Materials Research Diffractometer (MRD), at the UAF-AIL. The instrument utilized a CuKα source (45 kV and 40 mA), a Ni filter, 0.02 rad Soller slits, a one-half-degree divergence slit, and an *ÝCellerator* strip detector. The AD samples were scanned from 3° to 35° 2θ and the cation saturated samples (i.e., K + 550C, Mg + glycerol) from 4° to 20° 2θ, all with steps size of 0.01° 2θ at 0.06 s per step. The incident beam path had a nickel filter (0.02 mm thick), a soller slit with 0.02 opening rad., and an anti-scatter slit. Peak positions were assigned using the *PANalytical ÝPert* Data Viewer v1.2d and the mineral identification was done manually using (Chen, 1977) as reference.

2.3.2.2. Quantitative XRD of powder samples (<2 mm). The quantitative X-ray diffraction patterns (QXRD) of bulk samples were collected from powders packed into zero-background well holders using a *Rigaku SmartLab SE* diffractometer. It was employed a Bragg-Brentano geometry with a Cu X-ray source (λ = 1.5418 Å), a variable divergence slit, and a high-speed D/teX Ultra 250 1D detector. The samples were scanned between 2 and 100 °2θ at intervals of 0.01 °2θ, scanning at 2°2θ/min. The proportion of minerals was quantified by the Rietveld method using TOPAS (v6, Bruker AXS). This method combines calculated XRD patterns from the substituent minerals to provide the best fit with the observed pattern. For each mineral the scale factor, cell parameters (constrained within ca. 0.5 % of the expected values), and crystallite size (constrained between 50 and 500 nm) were refined. For platy minerals (e.g., mica minerals), a preferred orientation correction was also refined. The scale factors from the Rietveld refinement were used to determine the relative quantities of the minerals, which are presented scaled to a total of 100 %. Unidentified or amorphous compounds were ignored.

2.3.3. Fe and Al selective extractions

Selective Fe and Al extractions were performed on < 2 mm samples. Pedogenic Fe (Fe_d) was extracted by a dithionite-citrate-bicarbonate (DCB) solution (Mehra, 1958). DCB extraction is considered a measure of "free iron" in soils, solubilizing crystalline (e.g., goethite, hematite), and short-range-ordered (e.g., ferrihydrite) mineral (oids), as well as organometallic complexes. Al extracted by DCB is generally an estimate of Al substituted in Fe oxides (Schwertmann and Taylor, 1989). Short-range ordered (SRO) Fe and Al (oxy) hydroxides, including organometallic complexes, were extracted by ammonium oxalate solution (0.2 M, pH 3) (Fe_o and Al_o) (McKeague and Day, 1966; Schwertmann, 1964). Unlike Fe extracted by DCB, total pedogenic Al is better extracted by ammonium oxalate (Wada, 1977). Thus, Al extracted by ammonium oxalate represents the total pedogenic Al in soils, which is dominated by allophane, imogolite, and Al in organometallic complexes (Parfitt and Kimble, 1989; Wada, 1977). The organometallic complexes (Fe_p and Al_p) were extracted by a Na-pyrophosphate solution (0.1 M, pH 10) (McKeague et al., 1971).

The extracts (~10 mL) were measured in triplicates using a microwave plasma-atomic emission spectrometer (*Agilent 4200 MP-AES*) at the Water and Environmental Research Center, UAF. The instrument was set with a pump speed of 15 rpm, sample uptake time of 60 s, and stabilization time of 30 s. Multielement calibration standards (VeriSpec® Ricca Chemical Inc.) were used before the analysis and spiked samples (2.5 ppm) were included within the samples as a quality control check.

The data sets were used to calculate the proportions of crystalline, short-range ordered (SRO), and organometallic complexes. The values were also used to calculate the Al_o + ½ Fe_o ratio which is a taxonomic criterion for andic soil properties (Soil Survey Staff, 2014b). Values ≥ 2 % is one of the criteria for andic properties.

2.3.4. Electron microprobe analysis

Thin sections of spodic horizons were carbon-coated and analyzed with a JEOL electron microprobe at AIL-UAF, with an accelerating voltage of 15 kV and a beam current of 43 nAmps. Emphasis was given to point analysis and elemental maps of weathering features of individual mineral grains, rock boundaries and fissures, and neoformation/transformation of primary minerals.

2.4. Statistical analysis

Means and standard deviations of data were calculated with the software JMP Pro 15.2.0 (SAS, Cary, NC). We used ANOVA to test for the main effects of depth and lithology types on the analyzed soil properties. Paired means at the different depths and lithologies were also compared using the Tukey-Kramer HSD test, and simple linear regression was used. A heatmap indicating the Pearsońs correlation between the WISP against multiple soil properties: τ values of Si, Al, Fe, and base cations (i.e., K, Na, Ca, and Mg), soil texture, pH, and bulk density. For all statistical tests, a significance level of $p < 0.05$ was set as the alpha level.

3. Results

3.1. Soil morphology and classification

The pedons had similar morphology and horizons thickness (Table 2, Fig. 3). Although all pedons used in this study are representative of the region, we selected those having Andic properties (one pedon of each lithology) to display in Table 2 as this subgroup is considered the most developed Spodosol type in southeast Alaska (Alexander et al., 1993) the other pedons morphological properties are in the Supplementary Table 1. Pedons were generally thick (~100 cm), especially considering their locations on steep slopes averaging 50 %. The mean thickness of the organic horizon was 9.1 cm, without significant differences among lithologies. Organic horizons were mostly composed of poorly (Oi) to moderately decomposed plant materials (Oe) and a thick moss carpet, with high SOC content (>40 %). Transition to the E horizons was usually abrupt/clear and smooth. The E horizons were generally thin, averaging 7 cm, and often presented a wavy transition to carbon-rich Bh horizons. The overall high SOC content for the E horizons, from 3 to 9 %, indicated a mixing with organic horizons above and/or the Bh horizon underneath it.

The spodic horizons were generally composed of a thin Bh horizon overlying a thicker Bhs horizon, that gradually evolved to a Bs horizon. The spodic horizons were mainly separated by differences in color, with the Bh having darker colors, the Bhs a dark brownish color, and Bs with predominant light brown-reddish/orange colors. The average thickness of the spodic horizons was 15 ± 6 cm in phyllite, 18 ± 5.2 cm in metavolcanic, 22.5 ± 5.6 cm in tonalite, and 23 ± 5.2 cm in slate but was not significantly different among lithologies ($p > 0.05$). The transitions to the C horizons were usually gradual, and transitional BC horizons were frequently observed. A horizons were absent. Subangular blocky structure predominated, mostly medium in size, showing a trend of moderate to weak with depth. Blocky peds in the E horizons tended to become moderately indurated upon drying.

Despite the overall low bulk density, tonalite (average 0.58 g/cm^3) and metavolcanic (0.56 g/cm^3) were denser than phyllite (0.39 g/cm^3) and slate soils (0.33 g/cm^3). The textures were predominantly silt loam to loam, except in tonalite soils, which had a coarser sandy loam texture (Table 2). The sand and silt contents among phyllite, slate, and metavolcanic soils were relatively similar and significantly different ($p < 0.05$) compared to the tonalite (higher sand and lower silt content). Clay content had average values between 9 % and 15 % and without significant differences among the lithologies. The presence of rock fragments (> 2 mm) was common for all lithologies with an increasing trend with depth (Table 2).

The depth distribution of the different particle sizes exhibited similar trends and some disparities (Fig. 4). The sand particles were homogeneously distributed in the tonalite, with a slight increase in the C horizons. The depth distribution of sand in phyllite and metavolcanic soils was similar, with a clear increase towards the C horizon. In slate soils, sand concentrations increased in the spodic horizons. The silt content was much higher in the E horizons for all lithologies at approximately 60 %, except in the tonalite soils where the silt content was 22 %. The clay fraction had a more consistent distribution with depth (Fig. 4). In the slate and tonalite soils, the spodic horizons showed a subtle clay enrichment, and in the metavolcanic and phyllite soils, clay content was similar between the E and spodic horizons and slightly lower in the C horizons.

All pedons met the requirements for the Spodosol order and Cryic suborder (i.e., soils with a mean annual temperature between 0 and 8 °C without permafrost) (Soil Survey Staff, 2014a), having the presence of well-defined spodic horizons with pH < 5.9, SOC > 0.6 %, and color requirements (Table 2). The albic horizon (i.e., E horizon) was ubiquitous, except for one metavolcanic (i.e., P9V). Humicryods (SOC > 6 %) and Haplocryods (other Cryods) were the prevalent great groups. The Andic subgroup was attributed to 7 of the 11 pedons regardless of the parent material as defined by low bulk density (<0.9 g/cm^3) and Al + ½Fe_o content > 2 %. Thixotropic properties, with a typical smeary consistency, were observed in the more organic-rich spodic horizons. The Typic subgroup was noted for P2T and P9V, and the Lithic (lithic contact within 50 cm of mineral soil surface) for P3P and P9V.

The presence of one or multiple lithological discontinuities was detected in all lithologies in the field and using the UV index. The identification of lithological discontinuities was first based on field morphology by the presence of broken and buried horizons (i.e., E and/or spodic horizons), a sudden increase/decrease in large rock fragments, and/or abrupt textural change (Table 2, Supplementary Table 1). Next, the uniformity value (UV) index confirmed the presence of the discontinuities given that values exceeding 0.6 suggest a potential discontinuity (Cremeens and Mokma, 1986). In the studied soils, the most common occurrence of lithological discontinuities was often associated with UV values exceeding 0.6 (e.g., P6S – Bs – 2Cr, UV = 1.8). However, discontinuities were also identified between horizons with UVs < 0.6 (e.g., P1T – Bs – 2Bs, UV = 0.3) and in other cases, no apparent discontinuity was detected in the field even with high UV (e.g., P6S – E – Bh, UV = 1.6).

3.2. Mineralogical composition

The composition and proportion of primary minerals were different across the lithologies, but the weathering trend was similar (Table 3). The E horizons were strongly depleted in Mg-rich and K-rich minerals, chlorite, and muscovite, respectively. Albite (Na-plagioclase) was the main plagioclase in phyllite, slate, and metavolcanic soils while anorthite (Ca-plagioclase) dominated in tonalite soils. Both plagioclases followed a similar trend, with a progressive decrease from the C to the B horizons. Albite had a sudden increase in E horizons of phyllite, slate, and metavolcanic soils. Quartz also had a sharp increase in the E horizons of all lithologies. While it could be attributed to a residual enrichment, the concomitant increase of albite and silt (Section 3.1) suggests a potential aeolian addition of those minerals on the soil surface.

The proportion of Mg-Ca-rich minerals in metavolcanic soils was much higher than in the other lithologies. Hornblende, epidote, and pyroxene were present in significant proportions and did not show any clear weathering trend. These minerals were also present in lesser proportions in tonalite soils and insignificant proportions in phyllite and slate soils.

Overall, the most significant sources of base cations (Ca, K, Mg, and Na) for tonalite soils were anorthite > hornblende > albite > biotite > muscovite; for phyllite soils were albite > chlorite > muscovite; for slate soils were chlorite > muscovite > albite; for metavolcanic soils were hornblende > albite > chlorite > muscovite > epidote > pyroxene. Thus, these results demonstrate that metavolcanic soils have wider base-cations sources, and slate and phyllite the least. The most significant Fe source for tonalite soils was hornblende > biotite; for phyllite and slate soils was chlorite, and for the metavolcanic was hornblende > chlorite > epidote > pyroxene.

Table 2
Soil morphological, physical, and chemical properties of selected pedons (the remaining pedons are described on Supplementary Table 1).

Site/Pedon				Particle size distribution								Soil structure			Roots	
Horizon	Depth cm	Munsell color Moist	BD[1] g/cm[3]	RF[2] %	Sand[3] %	Silt[5] %	Clay[6] %	Texture[7]	UV index[8]	SOC[9] %	pH[10]	Grade[11]	Type[12]	Size[13]	Q[14]/S[15]	$Al_o + ½ Fe_o$[16] %
Tonalite																
P1T – Andic Humicryod																
Oi	0–20	2YR 2.5/1	0.6	–	–	–	–	–	–	46.6	3.8	–	–	–	3vf, f; 2 m,c	–
E	20–24	7YR 4/3	–	5	70	24	6	SL	0.2	7.5	4.0	2	SBK	m	2f, 2	–
Bh	24–27	10YR 2/1	–	10	67	22	11	SL	−0.1	13.1	3.8	2	SBK	m	2f; 3 m,c	–
Bh2	27–55	5YR 4/6	–	30	67	22	12	SL	0	6.0	5.2	2	SBK	m	1f, m	3.8
Bs	55–78	7.5YR 4/6	–	30	68	22	9	SL	0.2	5.4	5.2	2	SBK	m	–	–
2Bs	78–96	10YR 5/3	–	40	72	19	9	SL	0.3	5.9	5.1	1	SBK	c	–	–
2Bhs	96–110	10YR 3/3	–	50	75	15	10	SL	–	3.9	5.2	1	SBK	c	–	–
3C	110–135	2.5Y 4/2	–	–	–	–	–	–	–	1.2	5.2	–	MA	–	–	–
Phyllite																
P5P – Andic Humicryod																
Oi	0–5	2.5YR 2.5/2		–	–	–	–	–	–	–	3.8	–	–	–	3vf, f; 2 m	–
Oe	5–15	2.5YR 3/6	0.1	–	–	–	–	–	–	–	3.5	–	–	–	2f, c; 3 m	–
E	15–23	N 3/3	0.2	20	25	62	13	SiL	0.7	7.2	4.0	1	GR	f	1f, m	1.0
Bh	23–28	7.5YR 2.5/1	0.3	30	26	43	31	CL	0.2	10.3	4.1	1	SBK	m	–	2.5
Bhs/Bs	28–54	10YR 3/4	0.3	40	38	50	12	L	−0.2	6.6	4.7	2	SBK	m	–	3.0
2E	54–60	N 4/4	–	40	32	57	11	SiL	0.5	3.4	4.8	2	SBK	m	–	1.7
2BC	60–85	10YR 3/3	–	40	43	48	9	L	1.2	4.1	4.9	2	SBK/GR	m	–	2.4
3Bsg	85–112	2.5YR 4/3	–	65	59	34	7	SL	–	3.3	5.0	2	SKB/GR	m	–	2.6
3BCg	112–145	7.5YR 3/4	–	55	–	–	–	–	–	5.9	4.9	2	SBK/GR	m	–	3.3
Slate																
P8S – Andic Humicryod																
Oe	0–10	–	0.1	–	–	–	–	–	–	45.6	3.9	–	–	–	–	
E	10–16	5YR 6/1	0.3	55	43	50	7	SiL	0.5	4.9	3.7	–	MA (apedal)	–	–	0.6
Bh	16–26	5YR 2.5/2	0.2	–	46	36	18	L	0.1	15.3	4.1	2	SBK	–	f	2.7
Bhs/Bs	26–61	5YR 4/6	0.2	–	52	37	12	L	0.3	5.8	4.7	2	SBK/GR	–	vf	2.7
2Bs/C	61–92	7.5YR 5/4	0.2	–	58	32	10	SL	–	3.7	4.9	–	MA	–	–	2.3
2C	92–110	–	–	–	–	–	–	–	–	–	–	–	–	–	–	–
Metavolcanic																
P11V – Andic Haplocryod																
Oe	0–10	7.5YR 2.5/3	0.1	–	–	–	–	–	–	47.0	3.8	–	–	–	3vf, f; 2 m	–
E	10–14	7.5YR 5/3	0.5	–	31	64	5	SiL	0.6	3.5	4.1	1	GR	m	2f, m	0.7
Bh	14–20	7.5YR 2.5/1	0.6	–	36	54	10	SiL	0.1	9.0	4.0	2	SBK	m	1f, m	2.6
Bs1	20–60	5YR 4/6	0.6	–	39	54	7	SiL	0.5	3.3	5.0	2	SBK	m	–	2.5
Bs2	60–105	5YR 4/6	0.8	–	47	48	5	SL	0.9	1.3	5.3	2	SBK	m	–	1.8
2BC	105–158	5YR 3/4	–	–	63	34	3	SL	–	0.4	5.5	3	SBK	m	–	1.3
2C	158+	–	–	–	–	–	–	–	–	–	–	–	–	–	–	–

[4]VF = Very fine sand = 100–50 mm.
[1] BD = Bulk density.
[2] RF = Rock fragments. Material with a diameter > 2 mm.
[3] Sand = 2000–50 mm.
[5] Silt = 50–2 mm.
[6] Clay = <2 mm.
[7] Textural class – LS = Loamy Sandy, SL = Sandy Loam, SiL = Silt Loam, L = Loam.
[8] UV index = Uniformity value index (Cremeens and Mokma, 1986).
[9] SOC = Soil organic carbon.
[10] pH H_2O.
[11] Soil structure – Grade: 0 = Structureless, 1 = Weak, 2 = Moderate, 3 = Strong.
[12] Soil structure – Type: GR = Granular, SBK = Subangular blocky, MA = Massive.
[13] Soil structure – Size: VF = Very fine, F = Fine, M = Medium, C = Coarse.
[14] Roots – Quantity: 1 = Few, 2 = Common, 3 = Many.
[15] Roots – Size: VF = Very fine, F = Fine, M = Medium, C = Coarse, VC = Very coarse.
[16] $Al_o + ½ Fe_o$: Ammonium oxalate extraction of Fe and Al.

3.3. Clay mineralogy

The common primary mineral assemblage found in the clay fraction was composed mainly of quartz (d = 3.34 Å, 4.26 Å), mica (d = 10 Å, 5 Å, 3,33 Å), and plagioclase (d = 3.22 Å, 3.24 Å, 4.03 Å) (Table 4). Mica peaks were generally weak and gradually decreased moving upwards and represented the main weathering trend for all soils (Fig. 5). Chlorite, with reflections at d = ~14.2 Å, ~7.1 Å, 4.72 Å, 3.54 Å, and 2.82 Å, was more common in phyllite and slate soils and occurred in traces in one metavolcanic (P11V) and tonalite soil (P2T). Amphibole, with reflections at d = ~8.5 Å and ~3.13 Å, was present in the metavolcanic (actinolite) and tonalite (hornblende) soils and found in trace amounts in one phyllite soil (P4P) indicating potential contamination from other rock types.

The weathering of mica was identified by the decrease of its 001 reflection peak at d = 10 Å with a simultaneous broadening (often as doublets) and intensification of the peaks in the lower angle region near ~11.5 Å, ~12–13 Å, ~14 Å, and ~23–24 Å. The peaks were assigned as

Table 3
Quantitative mineralogical composition of bulk samples (<2 mm).

Pedon	Horizon	Depth (cm)	Quartz	Albite	Anorthite	Microcline	Chlorite	Muscovite	Biotite	Amphibole	Epidote	Pyroxene
			%									
P1T	E	20–24	41	4.5	31	4.4	1.1	2.4	1.7	8.8	1.0	1.4
	Bh	24–27	27	12	32	3.2	3.3	2.0	2.4	13	1.8	1.2
	Bh2	27–55	18	13	34	5.1	7.1	1.5	0.7	4.5	2.5	12
	Bs	55–78	33	1.7	42	3.7	1.9	3.0	0.6	7.1	3.6	3.1
	2Bs	78–96	31	8.4	38	2.8	2.3	3.2	2.3	6.7	3.1	1.2
	2Bhs	96–110	18	7.5	49	2.0	3.8	2.8	2.4	9.9	2.4	0.9
	3C	110–135	17	8.9	46	3.4	2.8	4.8	5.2	9.8	0.2	0.6
P3P	E	20–24	35	33	1.8	3.7	6.4	5.3	1.4	1.5	8.8	1.7
	Bhs	24–29	28	27	3.2	2.7	14	8.3	2.3	1.4	9.7	1.9
	B/C	29–37	28	28	4.5	3.8	18	8.4	2.3	1.1	3.9	2.5
P6S	E	5–13	55	20	0.8	0.1	6.3	12	1.1	0.3	1.1	1.7
	Bh	13–16	35	9.6	6.6	0.3	21	13	1.2	0.0	6.3	2.2
	Bhs	16–25	43	13	2.0	1.4	17	17	1.5	0.8	0.2	0.8
	Bhs2	25–42	43	13	2.5	2.8	17	17	1.7	0.9	0.1	0.8
	Bs	42–100	37	13	1.4	0.7	20	20	2.9	2.2	1.4	1.5
	2Cr	100+	31	18	0.0	1.2	24	22	0.8	0.7	1.0	0.8
P11V	E	10–14	6.2	34	6.8	2.7	2.1	2.7	1.3	25	17	0.9
	Bh	14–20	1.7	26	15	3.0	5.6	3.9	1.5	28	9.2	3.8
	Bs1	20–60	1.5	31	12	0.9	8,1	8.8	1.7	23	7.9	2.8
	Bs2	60–105	2.7	32	3.8	3.3	7.4	6.6	2.9	27	8.4	3.3
	2BC	105–158	1.5	32	4.2	2.9	8.5	8.4	1.3	27	8.0	4.8

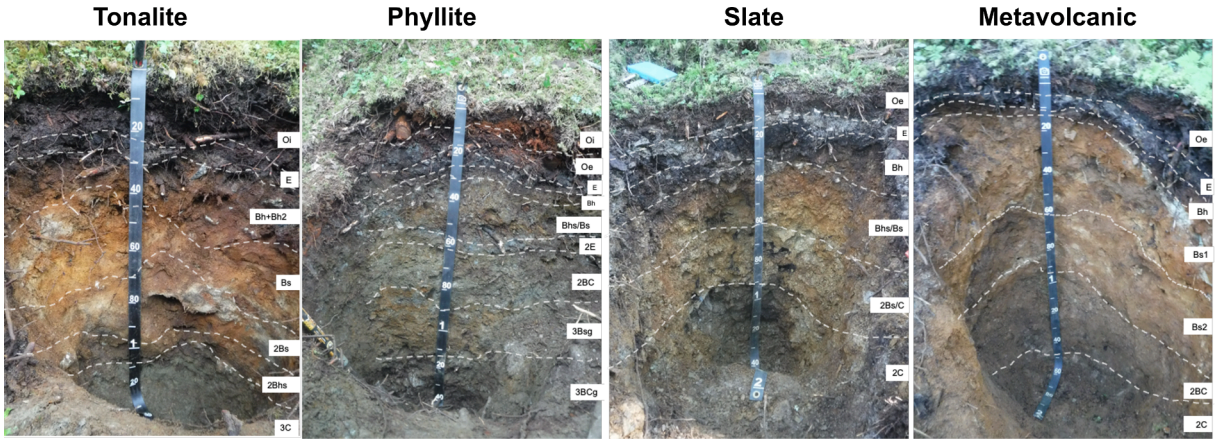

Fig. 3. Selected soil profiles of each lithology. Tonalite (P1T), Phyllite (P5P), Slate (P8S), and Metavolcanic (P11V).

interstratified mica-vermiculite minerals, such as muscovite-vermiculite and biotite-vermiculite (hydrobiotite) with a more micaceous component near 11.5–12 Å and more vermiculite layers near 13–14 Å. Interstratified mica-vermiculite was the most common clay mineral for all lithologies. Vermiculite was identified by a slight shift from a ~14 Å peak (AD), towards ~14.6 Å upon Mg + Gl and a collapse to ~10.5 Å after K + 550C (Fig. 6a).

Smectite was present as a three-component interstratified mica-vermiculite-smectite and was detected in the E horizons of all lithologies, except tonalite. Smectite was identified by an overall high-intensity peak around 12.3 Å (AD), which expanded to ~19 Å upon Mg + Gl and collapsed to ~10 Å after K + 550C (Fig. 6c, d).

Kaolinite was identified in all lithologies but only in traces in phyllite soils. It had broad, lower intensity peaks except for sharper peaks expressed in one slate soil (P8S). Kaolinite was identified by its basal reflection 001 and 002, at ~7.16 Å and 3.58 Å, respectively, which collapsed after K + 550C (Fig. 6a, c, d).

The presence of hydroxy interlayered minerals (HIM) is unlikely, but it was not eliminated for soils containing chlorite in the clay fraction because most of the vermiculite-smectite peaks did not fully collapse to 10 Å after K + 550C but remained between 10.2 and 10.5 Å. Only in two horizons (P5P-2E and P11V – Bs1), the identification of HIM was more likely due to the partial collapse to ~11.5 Å after K + 550C (Fig. 6b).

Tonalite soils exhibited a transformation from mica to vermiculite with interstratified vermiculite-mica as intermediate components (Fig. 5a). Kaolinite was present in both soils and had a sharper peak at P2T, particularly in the E horizon. Hornblende showed a relatively constant peak at P2T and a slight decrease upwards at P1T. Plagioclase peaks were weakly expressed and did not show a clear depth trend.

Phyllite soils also displayed a decrease of mica peaks towards the spodic horizons and a simultaneous increase of vermiculite layers (Fig. 5b). The presence of smectite in the E horizon of P3P is suggested due to the similarity of the peak shape and d spacing with the other smectites. However, no treatment was done with this sample to confirm. Low intensity kaolinite peaks were detected in only one horizon (P4P – 2Bhs). The peak corresponding to plagioclase had low intensity and showed a subtle decrease towards the soil surface.

Slate soils had a predominance of interstratified mica-vermiculite

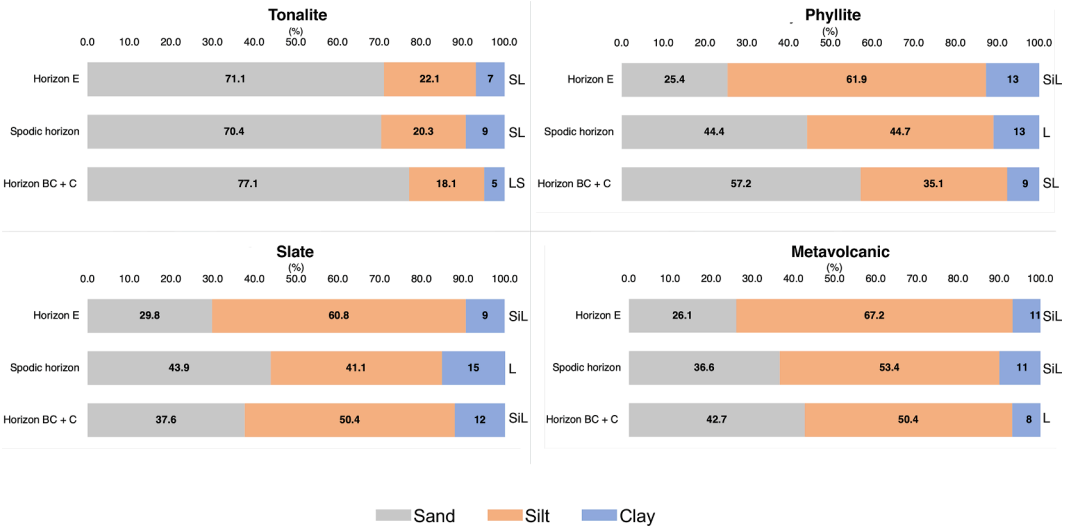

Fig. 4. Mean particle size distribution (%) in the E, spodic, and C horizons for each lithology type. Sand (50 - 2000 μm), silt (2 - 50 μm), and clay (< 2 μm). LS = Loamy Sandy, SL = Sandy Loam, SiL = Silt Loam, L = Loam.

(Fig. 5c). Smectite was identified only in the E horizons. The main difference between pedons P6S and P8S (data not available for P7S), was the sharp kaolinite peaks and faint chlorite peaks in P8S and the opposite in P6S, which had sharp chlorite and weak kaolinite peaks.

Metavolcanic soils shared similar trends for P10V and P11V but with different peak intensities (data not available for P9V) (Fig. 5d). Pedon P10V had weaker mica and sharp amphibole peaks. More prominent interstratified mica-vermiculite and vermiculite peaks were detected in the spodic horizons, while smectitic components appeared on the E horizons, even in the buried 2E horizon of P10V. Kaolinite peaks were broad and with poor intensity but more consistent through the P10V and only present on the E horizon of P11V.

3.4. Pedogenic Fe and Al (oxy)hydroxides

The average concentration of pedogenic Fe was much higher than Al for all lithologies (Fig. 7). Slate soils had the highest average Fe concentration in combined spodic and C horizons (44.5 ± 4.2 g/kg), followed by metavolcanic (31.6 ± 4.0 g/kg), phyllite (27.9 ± 3.8 g/kg), and tonalite soils (19.9 ± 5.7 g/kg). The concentration of pedogenic Al oxides in combined spodic and C horizons was not significantly different among the lithologies. Slate soils had slightly higher concentrations (11.2 ± 6.3 g/kg), followed by phyllite (10.7 ± 5.8 g/kg), tonalite (9.8 ± 9.0 g/kg), and metavolcanic soils (6.7 ± 3.5 g/kg).

The depth profile distribution of the crystalline ($Fe_d - Fe_o$), short-range ordered minerals (SRO, $Fe_o - Fe_p$), and the organometallic complexes (Fe_p) followed similar trends in all lithologies, with a lower concentration in the E horizons, a spike in the spodic horizons and a decrease in the C horizons (Fig. 8). The decrease of pedogenic Fe from the spodic to the C horizons was abrupt in all but the metavolcanic soils. Another major trend was the predominance of organometallic complexes in all horizons, especially in the spodic horizons. The crystalline species were the second most abundant and the SRO the least. The spodic horizons were dominated by organometallic species followed by crystalline phases. The SRO occurred mostly in E and C horizons but in minor amounts.

We also calculated the Fe crystallinity ratio, $Fe_{oxalate}/Fe_{dcb}$ (Supplementary Table 3). The ratio combines short-range-ordered minerals and organometallic complexes divided by pedogenic Fe, extracted by DCB. This ratio serves as a proxy for Fe crystallinity where values closer to 1 indicate a higher proportion of poorly crystalline species (e.g., ferrihydrite, organometallic complexes) and values closer to 0 indicate a higher proportion of more crystalline Fe species (e.g., goethite). The Fe crystallinity ratio confirmed the dominance of poorly crystalline species with mean values of 0.57 for slate soils, 0.64 for tonalite, 0.62 for metavolcanic, and 0.77 for phyllite soils. Only phyllite and slate soils had statistically significant differences, where slate presented the highest proportion of crystalline Fe phases among all lithologies (lower ratio).

The depth profile distribution of pedogenic Al was similar to Fe, with a lower concentration in the E horizon, a spike in the spodic horizon followed by a decrease in the C horizon (Fig. 9). This trend was noticed for all lithologies, except in the metavolcanic, which had a slightly higher concentration in the C horizon. In terms of fractionation, there was also a predominance of organometallic complexes over other pedogenic forms, which was more accentuated in the spodic horizons.

3.5. Geochemistry

The major elemental composition of the parent materials (averaged composition of C horizons) reflects the mineralogical assemblage (Table 5). The metavolcanic parent material is richer in Mg, Ca, Na, and Fe. On the other hand, slate is the poorest, and tonalite and phyllite are intermediate. The concentration of Fe was relatively high: 12.9 % in metavolcanic, 11.2 % in slate, 7.9 % in phyllite, and 6.9 % in tonalite. Despite not having the highest Fe concentration in the parent material, slate soils had the highest concentration of pedogenic Fe (section 3.4), indicating weathering of chlorite, which was the main and virtually the single Fe source in slate. Aluminum concentration was consistent across the parent materials, around 17 %, which was reflected in the similar concentration of pedogenic Al.

3.5.1. Weathering degree and mass balance

Average WISP values indicated that slate soils were the most depleted in base cations (WISP = 62 ± 8) and metavolcanic soils were the least (WISP = 45 ± 9.2) (Fig. 10). Phyllite (WISP = 55 ± 9.7) and tonalite soils (WISP = 53 ± 8.3) were intermediate. The depth profile trends are similar in all lithologies, with a subtle higher weathering degree in E horizons than in spodic horizons and the much less weathered C horizons. Only the metavolcanic soils did not show an abrupt difference between the solum (E + spodic horizons) and the C horizon. The spodic horizons were merged in the analysis because not all soils had a sequence of Bh-Bhs-Bs horizons. Nevertheless, there was a decreasing trend in the weathering degree from the upper part of spodic horizons down to the lowest horizons (Supplementary Table 2).

The open-system mass transport functions τ (tau) are reported as a

Table 4
Minerals in the clay fraction (<2 μm) of the investigated soil horizons.

		Clay minerals						Primary minerals				
Tonalite	Depth (cm)	Vm[1]	Sm[2]	Kt[3]	Mi-Vm[4]	Mi-Vm-Sm[5]	HIM[6]	Cl[7]	Mi[8]	Qz[9]	Plg[10]	Amp[11]
P1T – Andic Humicryod												
Bh2	27–55	(x)										
Bs	55–78	(x)										(x)
2Bs	78–96	x		(x)	x					x	x	(x)
2Bhs	96–110	x		x	x					(x)	(x)	(x)
3C	110–135	(x)		x	x				(x)	x	x	x
P2T – Typic Haplocryod												
E/B	3–18	x		x	x			(x)	x	x	x	x
Bs1	18–63	x		x	(x)			(x)	x	x	x	x
Bs2	63–90	x		x	x			(x)	(x)	(x)	x	(x)
2Cr	90–110	(x)		(x)	x			(x)	x	x	x	x
Phyllite	Depth (cm)	Vm[1]	Sm[2]	Kt[3]	Mi-Vm[4]	Mi-Vm-Sm[5]	HIM[6]	Cl[7]	Mi[8]	Qz[9]	Plg[10]	Amp[11]
P3P – Lithic Haplocryod												
E	20–24		likely		x	likely		(x)	(x)	x	(x)	
Bhs	24–29				x			x	(x)	x	(x)	
B/C	29–37				(x)			x	x	x	(x)	
P4P – Andic Haplocryod												
2Bhs	28–47				x			x	x	x	(x)	(x)
2B/C	47–55				x			x	x	x	(x)	(x)
3Bs	55–62				x			x	x	x	x	x
4C/B	62–87				(x)			x	x	x	x	x
4C	87+				(x)			x	x	x	x	x
P5P – Andic Humicryod												
E	15–23	x	(x)		x	(x)		x				
Bh (no data)	23–28											
Bhs/Bs	28–54				x			x	(x)	(x)	(x)	
2E	54–60	x			x		(x)	x	(x)	x	(x)	
2BC	60–85	(x)			x			x	(x)	(x)	(x)	
2Bsg	85–112				(x)			x	(x)	(x)	(x)	
3BCg	112–145							x	x	(x)	(x)	
4Cr	145+							x	x	(x)		
Slate	Depth (cm)	Vm[1]	Sm[2]	Kt[3]	Mi-Vm[4]	Mi-Vm-Sm[5]	HIM[6]	Cl[7]	Mi[8]	Qz[9]	Plg[10]	Amp[11]
P6S – Andic Humicryod												
E	5–13		x	(x)	x	x		x	(x)	x	x	
Bh	13–16			(x)	(x)			x	x	x	x	(x)
Bhs	16–25				(x)			x	(x)	(x)	(x)	
Bhs2	25–42	(x)			(x)			x	(x)	(x)	(x)	
Bs	42–100	(x)			(x)			x	(x)	x	(x)	
P8S – Andic Humicryod												
E	10–16		x	x	x	x			(x)	x	(x)	
Bh	16–26	(x)		x	x			(x)	(x)	x	(x)	
Bhs/Bs	26–61	(x)		x	(x)				(x)	(x)	(x)	
2Bs/C	61–92	x		x	x			(x)		x		
Metavolcanic	Depth (cm)	Vm[1]	Sm[2]	Kt[3]	Mi-Vm[4]	Mi-Vm-Sm[5]	HIM[6]	Cl[7]	Mi[8]	Qz[9]	Plg[10]	Amp[11]
P10V – Typic Humicryod												
E	5–9		x	x	(x)	x			(x)	x	(x)	x
Bhs	9–21	x		(x)	x				(x)	x	(x)	x
Bs	21–41	x		x	x				(x)	x	(x)	x
2E	41–55		x	x		x			(x)	x	x	x
3BC	55–105	x		x	x				(x)	x	(x)	(x)
3C	105+	(x)		(x)	(x)				x	x	(x)	x
P11V – Andic Haplocryod												
E	10–14	x	(x)	(x)	(x)	x			(x)	x	x	x
Bh	14–20				x			(x)	(x)	x	x	x

(*continued on next page*)

Table 4 (*continued*)

Tonalite	Depth (cm)	Clay minerals						Primary minerals				
		Vm[1]	Sm[2]	Kt[3]	Mi-Vm[4]	Mi-Vm-Sm[5]	HIM[6]	Cl[7]	Mi[8]	Qz[9]	Plg[10]	Amp[11]
Bs1	20–60	x			(x)		(x)	(x)		(x)	(x)	(x)
Bs2	60–105	x			(x)			(x)	(x)	x	(x)	x
2BC	105–158	(x)			(x)			x	x	x	x	x

[1]Vm = Vermiculite; [2]Sm = Smectite; [3]Kt = Kaolinite; [4]Mi-Vm = interstratified mica-vermiculite; [5]Mi-Vm-Sm = interstratified mica-vermiculite-smectite; [6]HIM = Hydroxy-interlayered minerals; [7]Cl = Chlorite; [8]Mi = Mica; [9]Qz = Quartz; [10]Plg = Plagioclase; [11]Amp = Amphibole. (x) = of minor importance.

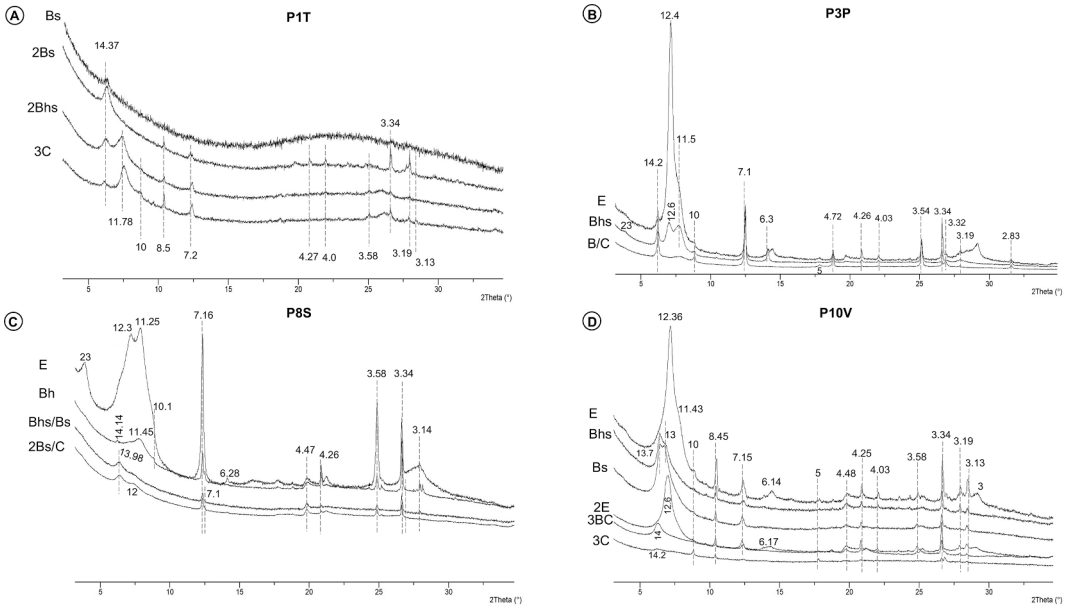

Fig. 5. XRD patterns of air-dry oriented mounts of the < 2 μm fraction for a representative pedon of each lithology. d-spacing values in Ångstroms (Å).

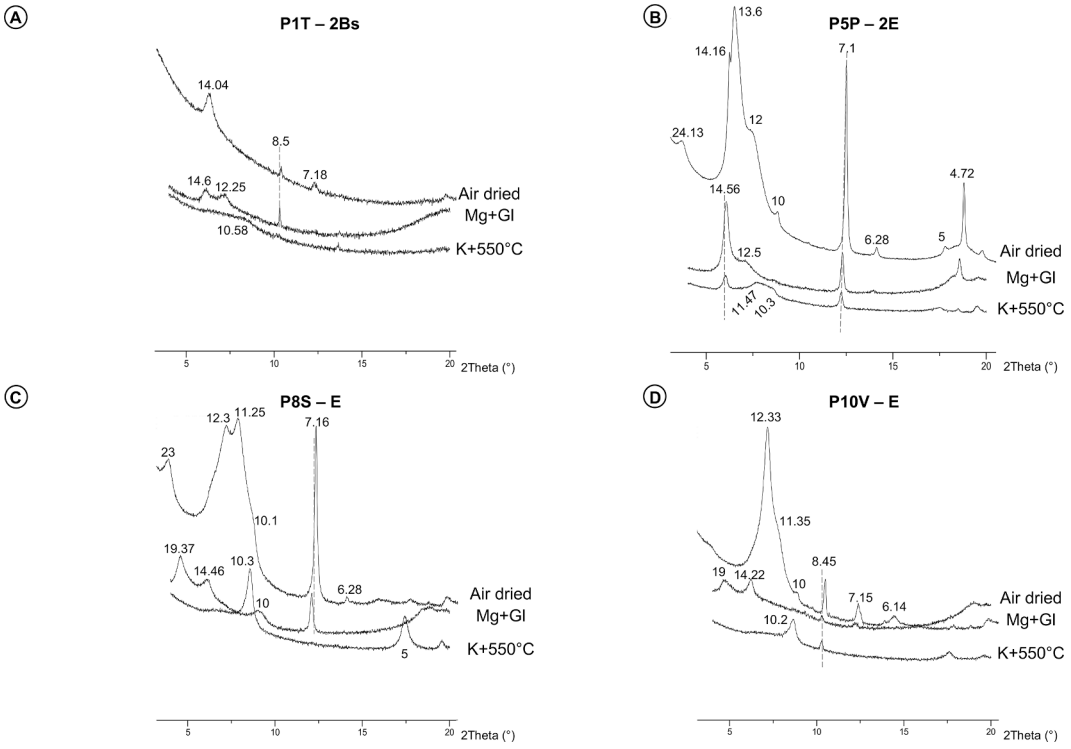

Fig. 6. XRD patterns of air-dry, Mg saturation and glycerol solvated (Mg+Gl), and K saturation followed by 550°C heating (K+550°C) oriented mounts of the < 2 μm fraction. d-spacing values in Ångstroms (Å).

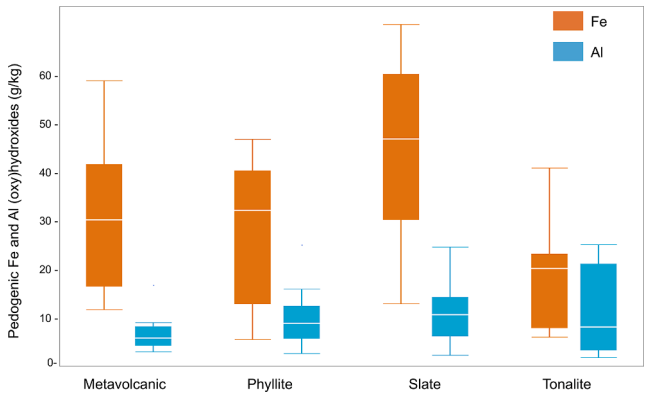

Fig. 7. Mean concentration (g/kg) of pedogenic Fe (orange bars) and Al (blue bars) of combined spodic and C horizons for each lithology. Pedogenic Fe was extracted by dithionite-citrate-bicarbonate solution and Al by ammonium oxalate solution. In the box plots, the center lines represent the medians, the box limits represent the interquartile ranges, the whiskers represent the quartiles plus 1.5x the interquartile range and closed circles represent outlying values.

function of lithology with average values for E and spodic horizons (Fig. 11, Supplementary Table 2). Overall, Mg, K, and Ca were the most depleted elements, followed by Na, Al, and Si. The main losses in the E horizons were K, Mg, Fe, and Al. In the spodic horizons, the main losses were Ca, Mg, Na and K. When the E horizon and spodic horizons are compared, K and Mg were lost more severely from the E horizon whereas Na and Si were more depleted from the spodic horizons. The differences in Ca losses between E and spodic horizons were only noticeable in slate, where it was more depleted in the spodic horizon. As expected, Fe was strongly removed from the E horizons and stable or enriched in the spodic horizons, most notably in slate soils (spodic τ Fe = 0.42) (Fig. 12). Aluminum was depleted similarly across all lithologies, more notably in the E horizons but it was also depleted from the spodic horizons, suggesting that Al is more soluble than Fe in these soils (Fig. 12). Except for tonalite soils, Si was virtually stable in E horizons of phyllite, slate, and metavolcanic soils despite clear silicate weathering.

The overall base depletion reflected the differences seen in the WISP, where slate soils were the most weathered, followed by phyllite, tonalite, and metavolcanic soils. However, there were no statistically significant differences ($p > 0.05$) for most elements, except Ca and Mg. Calcium depletion was stronger in phyllite (τ Ca = −0.52), which was significantly different only from metavolcanic soils (τ Ca = −0.22). Magnesium was more strongly depleted from tonalite (τ Mg = −0.62) with significant differences only compared with metavolcanic soils (τ Mg = −0.28).

The Fe_{dcb}/Fe_{total} ratio values indicate a stronger weathering of Fe-bearing minerals in slate, likely chlorite (Supplementary Table 4). A ratio close to 1 indicate higher weathering of Fe-bearing minerals and values close to 0 indicate lower weathering. The values were 0.19 for tonalite soils, 0.25 for phyllite and metavolcanic and 0.33 for slate soils.

Fig. 13 displays a heatmap where the WISP is correlated with the τ values of the major elements and several soil properties (i.e., SOC, bulk density, particle size distribution, and pH). The WISP had a significant positive correlation with SOC ($r^2 = 0.5$) and clay content ($r^2 = 0.5$). It had a negative correlation with bulk density ($r^2 = -0.6$), τ Ca ($r^2 = -0.6$), τ K ($r^2 = -0.5$), and particularly with τ Mg ($r^2 = -0.8$). The τ values of the other elements, such as Al, Fe, Na, and the other soil properties had a weak or no correlation with the WISP. Thus, it indicates that high SOC concentration, and depletion of Mg, Ca, and K played a major role in the weathering status.

3.6. Microscopic weathering features

Individual mineral weathering features were more commonly detected in the porphyritic rock types (i.e., tonalite and metavolcanic), whereas weathering features on fine-grained rocks (i.e., slate and phyllite) were most visible on rock fragments.

Different stages of biotite weathering were detected visually, from fresh to heavily altered, particularly on tonalite, which has larger biotite crystals (Fig. 14a). The observed biotite weathering usually started from the edge inwards. Fine-grained mica dispersed in the soil groundmass was more commonly detected on phyllite and slate (Fig. 14b). Amphibole weathering in tonalite soils and pyroxene weathering on metavolcanic soils appeared to have been a dissolution-precipitation reaction, in which minerals were partially dissolved and the weathering products reprecipitated on mineral cavities and surfaces (Fig. 14c, d). These weathering products were usually fine-grained Al or Fe-rich precipitates.

Rock fragment surfaces also provided microsites for element precipitation, chiefly Al, and Fe, often accompanied by carbon (C). These precipitates were detected within rock fissures (Fig. 15a) and on rock

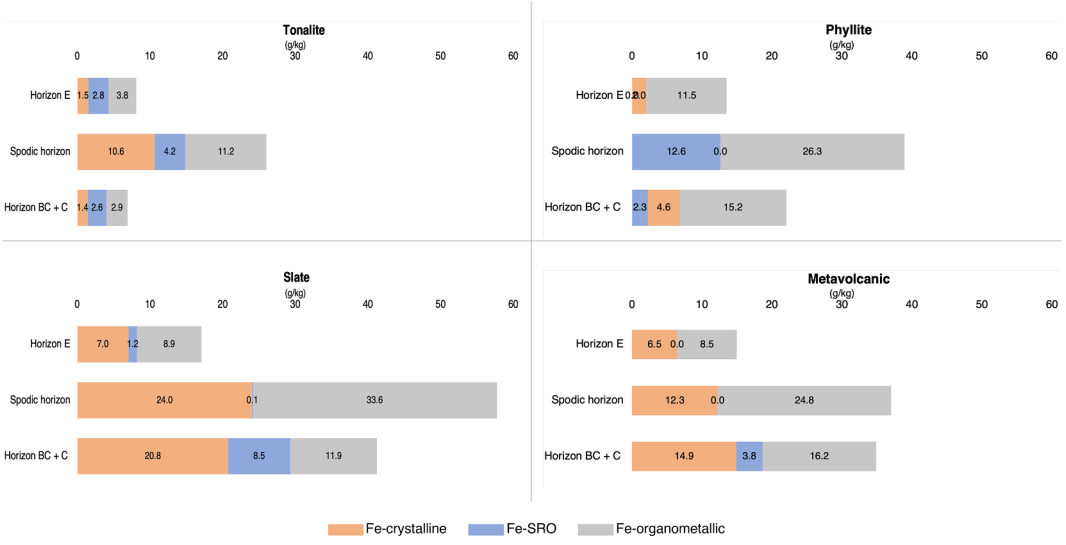

Fig. 8. Mean concentration (g/kg) of different species of pedogenic Fe in the E horizons, spodic horizons, and C horizons for each lithology. Fe-crystalline (orange bars) represents Fe extracted by dithionite-citrate-bicarbonate minus Fe extracted by ammonium oxalate; Fe-SRO (blue bars) represents Fe extracted by ammonium oxalate minus Fe extracted by Na-pyrophosphate and; Fe-organometallic (grey bars) represents Fe extracted by Na-pyrophosphate.

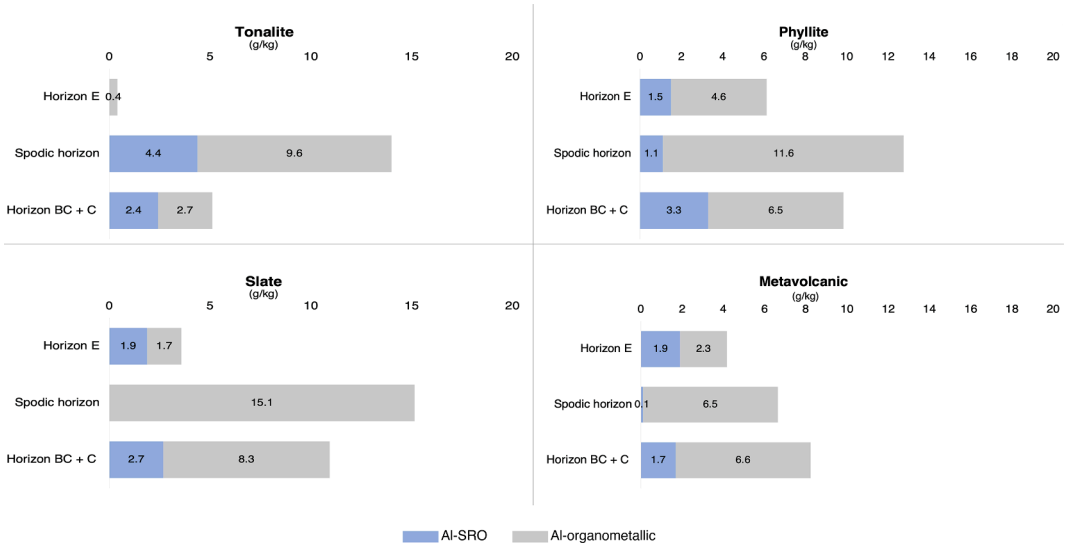

Fig. 9. Mean concentration (g/kg) of different forms of pedogenic Al in the E horizons, spodic horizons, and C horizons for each lithology. Al-SRO (blue bars) represents Al extracted by ammonium oxalate minus Al extracted by Na-pyrophosphate and; Al-organometallic (grey bars) represents Al extracted by Na-pyrophosphate.

Table 5
Average major elements composition of parent materials, corrected for loss on ignition.

Lithology	SiO_2 %	TiO_2	Al_2O_3	Fe_2O_3	MgO	CaO	Na_2O	K_2O
Tonalite	62 ± 3.7	1.1 ± 0.1	17.2 ± 1.3	6.9 ± 1.1	3.2 ± 0.7	4.3 ± 0.6	2.5 ± 0.2	2.1 ± 0.3
Phyllite	62.5 ± 10.1	0.9 ± 0.3	16.7 ± 5.3	7.9 ± 3.3	3.5 ± 1.6	3.2 ± 2.0	2.1 ± 0.7	2.5 ± 1.6
Slate	62.2 ± 6.7	0.9 ± 0.1	18 ± 1.9	11.2 ± 2.8	2.1 ± 1.3	0.4 ± 0.4	1.5 ± 0.6	2.3 ± 0.3
Metavolcanic	50.8 ± 1.8	1.2 ± 0.2	17.4 ± 3.7	12.9 ± 3.1	6.2 ± 2.2	6.2 ± 0.7	2.9 ± 0.4	1.5 ± 1.0

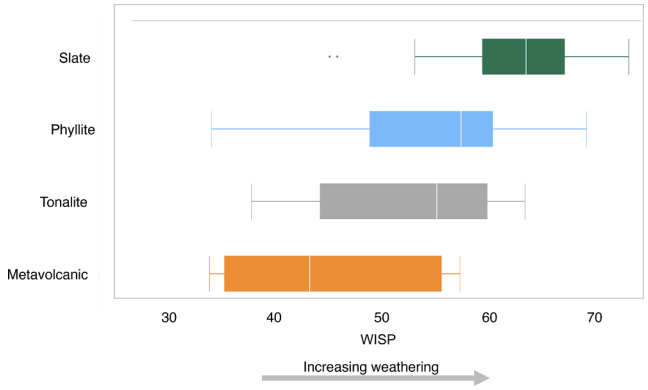

Fig. 10. Weathering Index for Spodosols (WISP) for each lithology. In the box plots, the center lines represent the medians, the box limits represent the interquartile ranges, the whiskers represent the quartiles plus 1.5x the interquartile range and closed circles represent outlying values. Averages represent the total number of samples per lithology: tonalite soils (n = 12), phyllite soils (n = 18), slate soils (n = 16), metavolcanic soils (n = 15).

edges, forming weathering rinds. The weathering rinds usually presented a rock-smectite-Fe(oxy)hydroxide (Fig. 15b) or a rock-Fe(oxy) hydroxide interface (Fig. 15c).

4. Discussion

4.1. The role of bioclimatic conditions on podzolization

The strong positive correlation between SOC content and the index of weathering (WISP) supports the conclusion that the regional bioclimatic conditions enhance chemical weathering. Weathering of primary minerals is influenced by the loss of nutrients through plant uptake, hydrologic loss of mobile elements, and podzolization processes in response to the presence of organic ligands facilitating the release of di- and trivalent metals (mainly Fe and Al) from phyllosilicates forming strong organo-metallic complexes (Balland et al., 2010; Buurman and Jongmans, 2005; Mokma and Buurman, 1987).

Despite the enhanced weathering response to bioclimatic conditions, high Fe concentrations and the relative fine texture of the soils likely prevented the formation of thick E horizons. The presence of thick E horizons is more common on sandy, Si-rich, Fe-poor Spodosols, where soluble organometallic compounds percolate deeper until reaching a certain pH and C/Fe ratio precipitation point (Duchaufour and Souchier, 1978; Ferro-Vázquez et al., 2020; McKeague et al., 1983; Sanborn et al., 2011). The Fe concentration in the parent material reported in this study exceeded by far the limits for podzolization in other temperate regions in Central Europe. Here, the Fe concentration values in the parent materials ranged from 7.9 % to 12.9 % while in Central Europe, Fe concentration ranges from 2 % to 5 %, which are considered thresholds for podzolization (Duchaufour and Souchier, 1978; Musielok et al., 2021; Sommer et al., 2000).

The weathering of chlorite, biotite, and to a lesser degree, ferromagnesian minerals (mainly on metavolcanic parent material) provided an abundant supply of Fe in all soils. High Fe concentration is considered as a limiting factor for podzolization (Duchaufour and Souchier, 1978; Musielok et al., 2021). However, podzolization of Fe-rich parent materials has been reported in other areas of the Pacific coastal temperate rainforests of North America (Alexander et al., 1994, 1993; Bulmer and Lavkulich, 1994; Sanborn and Lavkulich, 1989). Therefore, environmental conditions such as cool temperatures, abundant precipitation, and good soil drainage provided by the abundant rock fragments and

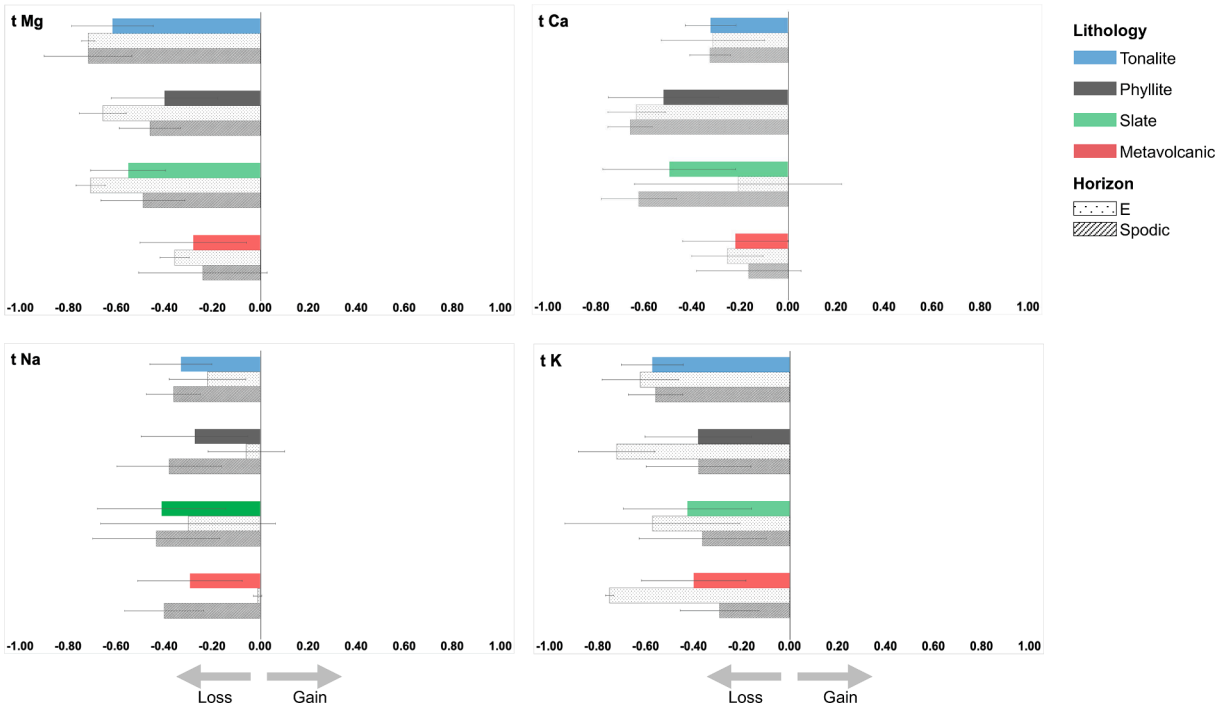

Fig. 11. Mass balance *(τ)* values of base cations (Na, Kg, Mg, and Ca) for all horizons (colored bars), E horizons (dotted bars), and spodic horizons (dashed bars) for each lithology. Blue bars = tonalite soils, grey bars = phyllite soils, green bars = slate soils, red bars = metavolcanic soils. Error bars represent standard deviation.

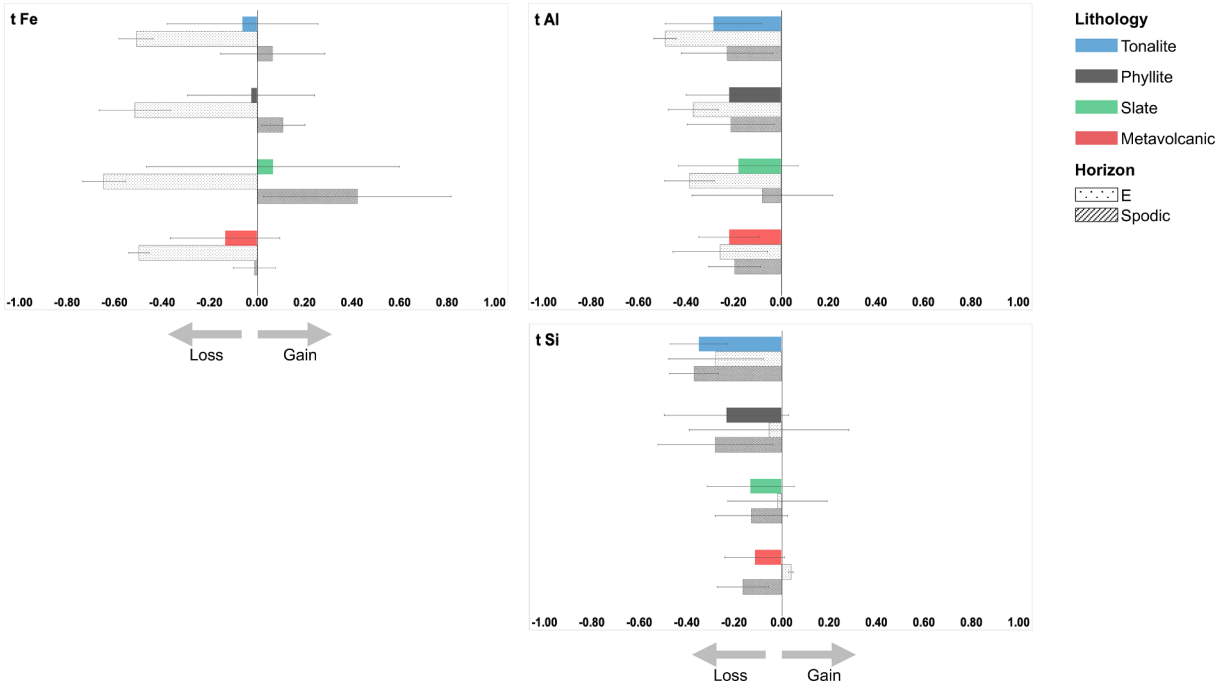

Fig. 12. Mass balance *(τ)* for Fe and Al for all horizons (colored bars), E horizons (dotted bars), and spodic horizons (dashed bars) for each lithology. Blue bars = tonalite soils, grey bars = phyllite soils, green bars = slate soils, red bars = metavolcanic soils. Error bars indicate standard deviation.

steep slopes, enhance the podzolization process, which can overcome the high Fe contents of parent materials (Alexander et al., 1994). Another factor is the low decomposition rates of coniferous vegetation, increasing the C/Fe ratio in the surficial horizons, at the contact between the O and the E horizon, promoting the translocation of organometallic complexes to the spodic horizons (McKeague et al., 1983). Thus, podzolization in coastal temperate rainforests can take place in soils with higher Fe, finer textures, and higher base-cations concentrations than in other temperate zones due to conditions of high leaching and cool temperatures.

4.2. *Mineral weathering and secondary phase distribution*

The most common mineralogical transformation for all lithologies was the dissolution of chlorite to Al-Fe-(oxy)hydroxides and a stepwise weathering of mica to interstratified clay mineral phases. The absence of

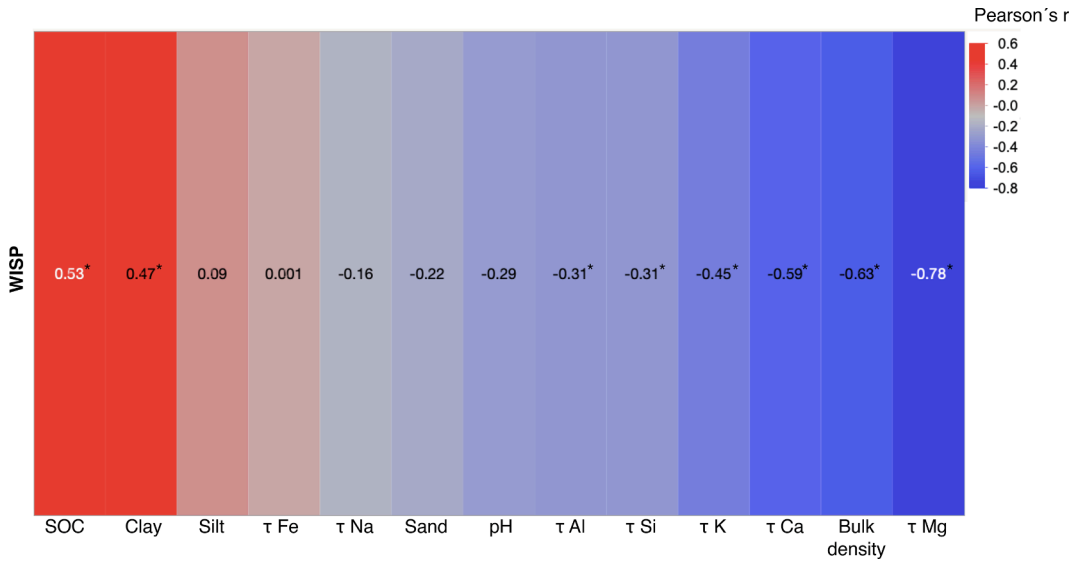

Fig. 13. Heatmap showing correlations between WISP and soil properties and elemental depletion values (. The color and numbers shown indicate the strength and sign of the correlation. Stronger reddish hues indicate a positive correlation and stronger bluish hues indicate a negative correlation. Significance of the correlations (*) is evaluated at $p < 0.05$.

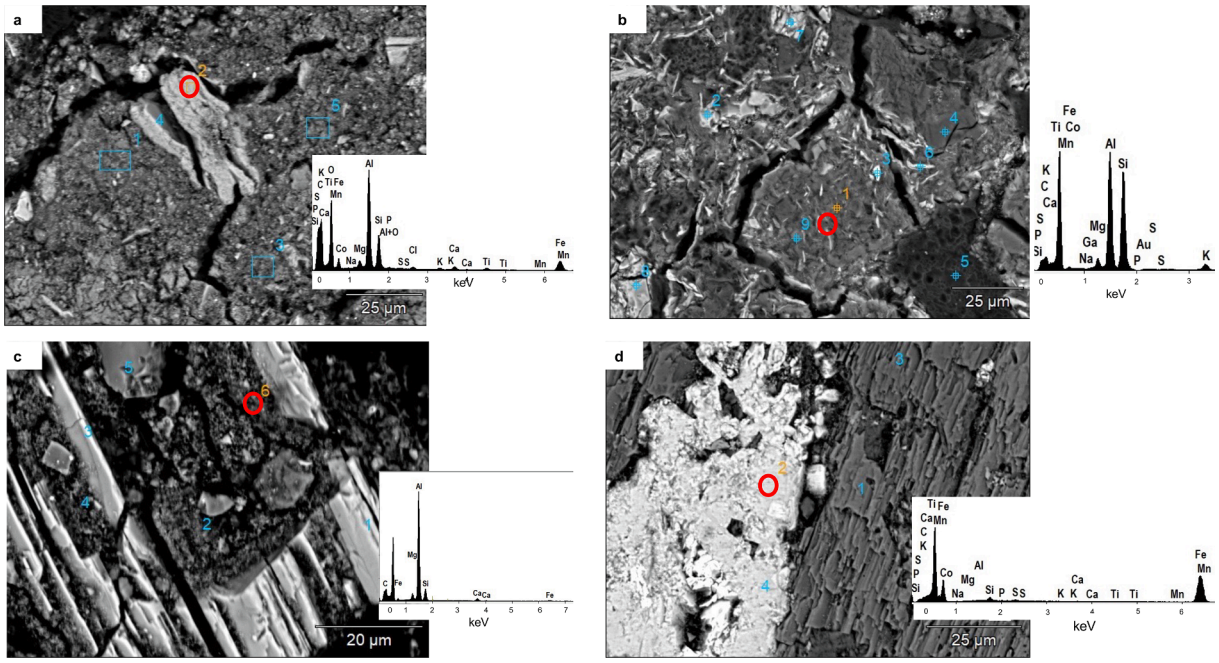

Fig. 14. Microprobe images of weathering of primary minerals. Red circles indicate where the displayed EDS data was taken. Blue numbers and squares contain data that are not shown here. a) a weathered mica grain from a tonalite pedon; b) fine-grained mica embedded in soil groundmass from a phyllite pedon: c) Al-rich precipitates on amphibole cavities from a tonalite pedon; d) Fe-rich precipitates on pyroxene cavities from a metavolcanic pedon.

intermediate chlorite weathering products in E horizons together with a strong loss of Fe and Mg indicates that chlorite has been dissolved (Bain, 1977; Wilson, 2004). Chlorite was the most susceptible mineral to weathering and occurred in abundance in slate soils, which is the reason why slate soils had the higher pedogenic Fe concentration among all lithologies. The stronger weathering intensity and less abundant supply of Fe-rich minerals suggest lower weathering rates for slate soils, which might also explain the higher Fe crystallinity (Slessarev et al., 2022). Metavolcanic soils were formed on a parent material with the highest Fe concentration, but Fe was distributed in minerals less susceptible to weathering than chlorite.

The further transformation of mica (muscovite and biotite) and mica-vermiculite to smectite in E horizons were enhanced by the loss of Fe and K, which is catalyzed by organic ligands that mobilize Fe from the E to the spodic horizons (Courchesne et al., 1996; Gillot et al., 2000; Kitagawa, 2005; Lundström, 1993). The formation of smectite due to stronger depletion of Fe and K in E horizons of Spodosols has been reported for other temperate regions as well (Egli et al., 2001; Mirabella et al., 2002; Waroszewski et al., 2016). The presence of a three-component random interstratified mica-vermiculite-smectite in this study highlights that transformation is the main process for smectite formation, commonly observed in most Spodosols, as opposed to

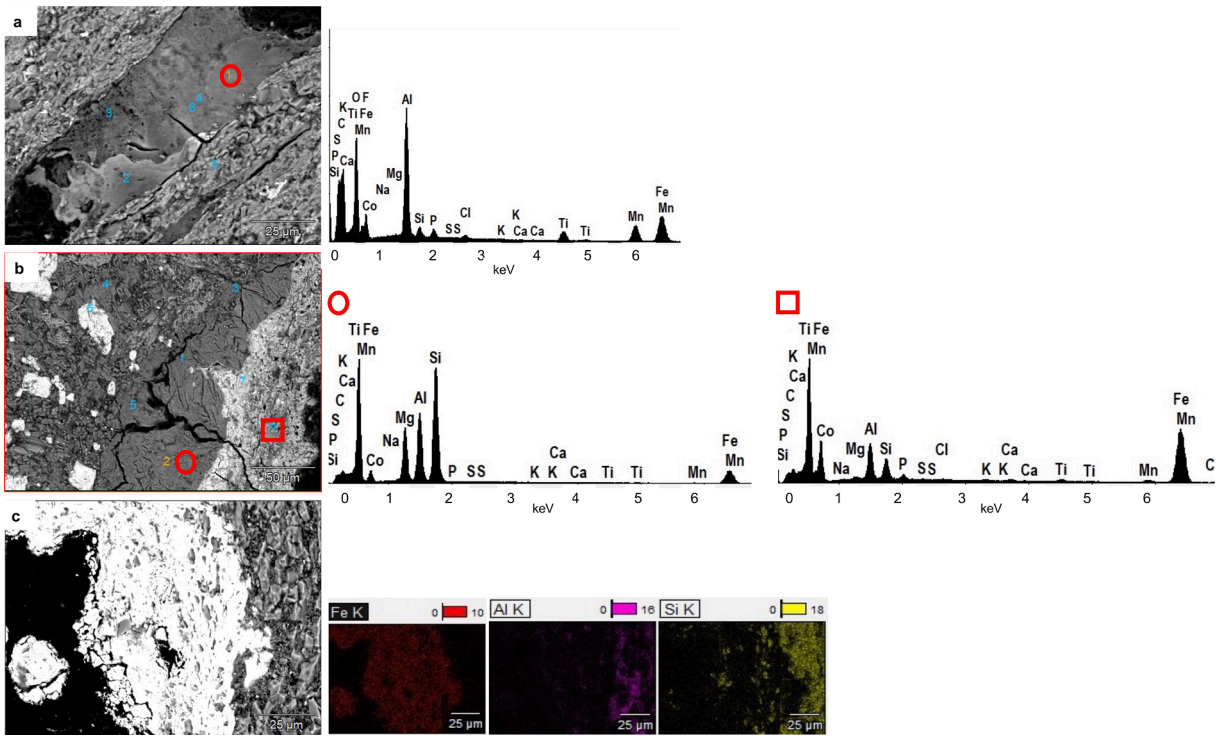

Fig. 15. Microprobe images of weathering of rock fragments. Red circles and squares indicate where the displayed EDS data was taken. Blue numbers contain data that are not shown here. a) an Al-rich precipitate within slate fissures; b) a weathering rind with a sequence, from left to right, a fresh metavolcanic rock - Mg-rich smectite and a Fe-rich coating; c) a Fe-rich weathering rind coating a slate fragment. The color intensity of the elemental maps indicates the relative Fe, Al, and Si concentration.

neoformation from soil solution (e.g., Vertisols) and/or inheritance from the parent material (e.g., Entisols) (Wilson, 1999).

Another pathway for the formation of smectite and vermiculite endmembers is through chlorite weathering. However, the absence of intermediate phases such as hydroxy-interlayered minerals (HIM) suggests chlorite has been mostly dissolved (Barnhisel and Bertsch, 1989; Wilson, 1999). In general, HIM are relatively stable, commonly identified as intermediate clay mineral phases (Barnhisel and Bertsch, 1989) but only detected in two samples. This supports the lack of HIM formation due to low pH, high SOC, and the predominance of pedogenic Al as organometallic complexes that inhibits HIM formation (Meunier, 2007).

Increased losses of Ca and Na in the spodic horizons suggest more intense plagioclase weathering, which is also supported by the formation of kaolinite. Although kaolinite is considered uncommon in Spodosols (Egli et al., 2001) it has been widely reported (Mirabella et al., 2002; Skiba, 2001; Waroszewski et al., 2016). In tonalite and metavolcanic soils, the presence of kaolinite is likely due to partial weathering of plagioclase, amphibole, and/or pyroxene (Egli et al., 2001; Velbel, 1989). Plagioclase, amphibole, and pyroxene were partially weathered followed by a non-stoichiometric reprecipitation of secondary phases on crystal cavities and surface coatings, which is a documented route of kaolinite neoformation (Inskeep et al., 1993; Velbel, 1989; Wilson, 2004). The sharp kaolinite peaks in the E horizon of slate indicated a further transformation from vermiculite-smectite, rather than neoformation.

We suggest the following mineral alteration sequence for the studied soils, regardless of the lithology:

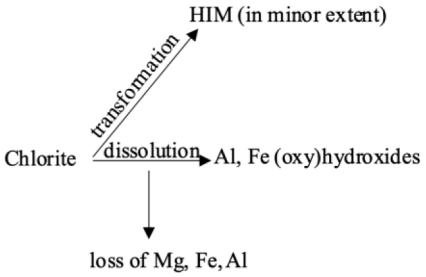

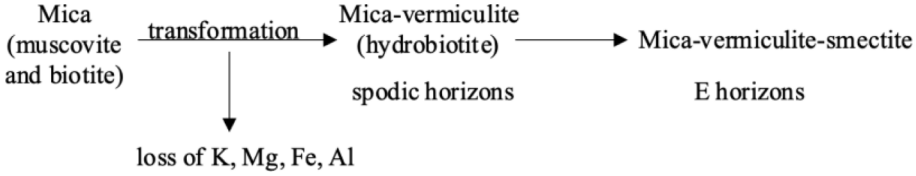

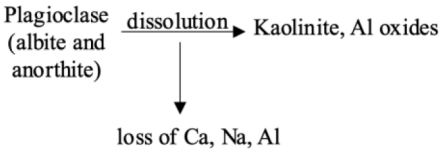

4.3. Relationship of weathering products to SOC

The dominance of Fe and Al-organometallic complexes in the spodic horizons for all lithologies suggests most of the organic matter might have been co-precipitated and/or adsorbed to Fe/Al oxides. Our recent data demonstrate that SOC stocks are similar across these lithologies in southeastern Alaska Spodosols (Fedenko et al., in review). Over 70 % of total SOC stocks are in the spodic horizons (Fedenko et al., in review) and most of this pool is associated with secondary minerals (Fleiner et al., in preparation), in line with global estimates for temperate rainforests (Kramer and Chadwick, 2018). It suggests that despite the significant role that secondary minerals play in SOC dynamics, the differences in pedogenic Fe oxide concentration found in this study were not sufficient to result in contrasting SOC stocks but the influence on SOC stability is unclear.

The higher proportion of organometallic complexes in spodic horizons was followed by more crystalline forms (e.g., nano-goethite). The formation of organometallic complexes lowers the activity of free Fe (i.e., non-complexed) leading to the formation of crystalline Fe in spodic horizons (Schwertmann et al., 1986; Shoji et al., 1993). Although more evidence is needed, we suggest these soils have not reached their C saturation point, and additional organic matter inputs can be retained by the existing non-complexed Fe and Al surplus.

The distribution and speciation of pedogenic Al were also related to podzolization, with abundant organometallic complexes of Al. However, Al had considerable net depletion compared to Fe based on the mass-balance calculations, consistent with observations in other Spodosols (Egli et al., 2004; Musielok et al., 2021). The net Al depletion suggests that Al is more soluble than Fe (Ferro-Vázquez et al., 2014; Jansen et al., 2003; Nierop et al., 2002) under the pH and metal/carbon ratios found in the Alaskan Spodosols.

4.4. Lithological influence on soil weathering intensity

The extensive leaching of major base cations from all horizons, and Fe and Al from E horizons were controlled by the primary mineral composition of the studied lithologies. The weathering of chlorite, mica, and plagioclases was the most common source of base depletion (mostly Mg, K, and Ca) across all lithologies. In particular, the main sources of Mg (chlorite) and K (mica) in the E horizons of phyllite and slate soils are virtually depleted, with unknown impacts on forest productivity. Enrichment of silt, quartz, and albite in E horizons of phyllite, slate, and metavolcanic soils suggest a potential dust deposition. Local glacial sediments are the most likely dust source because there are no other regional sources. Nevertheless, more evidence is needed to confirm the deposition of dust, its sources, and the potential implications for soil processes.

Slate soils were the most depleted in bases, followed by phyllite, tonalite, and metavolcanic soils. The pre-weathered nature of slate and phyllite, having shales as a protolith, produced soils with less diversity of base-rich minerals compared to tonalite and metavolcanic soils that are richer in base-rich minerals such as amphibole, pyroxene, and epidote. Thus, the more diverse mineral assemblage of tonalite and metavolcanic parent materials resulted in less weathered soils. In addition, the higher bulk density of the metavolcanic soils suggests that bases are not leached as rapidly as the other lithologies.

The use of the WISP index, using Ti as the immobile element, provided an indicator for Spodosol weathering in our environment due to the abundant leaching of Al. Weathering indices using Al as the immobile element, such as the CIA (Nesbitt and Young, 1982) have been occasionally used for measuring weathering in Spodosols (Vasyukova et al., 2019; Nelson et al., 2021). The CIA relies on the weathering of feldspars and the immobility of Al. However, our mass balance calculations indicated a strong Al mobility due to podzolization, hampering the reliability of the CIA. The (K + Ca)/Ti index was primarily developed as a dating method for rock varnish in desert regions (Dorn, 1983; Harrington and Whitney, 1987), but has been applied to evaluate Spodosol weathering (Dahms et al., 2012; Musielok et al., 2021; Waroszewski et al., 2016). Despite the advantage of using Ti as the immobile element, it uses only K and Ca as mobile elements. Our results showed that, in addition to Ca and K, Mg and Na were also strongly depleted, which limited the utility of the (K + Ca)/Ti index.

The potential mobility of Ti in soils by clay translocation has been reported (Chapman and Horn, 1968; Sudom and Star, 1971) as well as intense weathering under tropical conditions (Cornu et al., 1999). In those situations, Zr was indicated as the most stable element but low Zr concentration in soils can limit its reliability due to potentially larger analytical errors (Stiles et al., 2001; Sudom and Star, 1971). In this study, like most Spodosols in temperate forests, there is no clay translocation nor strong weathering comparable to tropical conditions. Moreover, the use of Ti as the immobile element in mass balance calculations is widely accepted and used for Spodosols elsewhere (e.g., Waroszewski et al., 2016; Egli et al., 2001, 2003, 2004; Lichter, 1998). We therefore suggest the adoption of WISP to evaluate the weathering degree of Spodosols, or any base-rich soil with Al mobility after an assessment of potential Ti mobilization.

4.5. Steady-state conditions of Spodosols in southeast Alaska

Constraining soil age in southeast Alaska is facilitated at the maximum by the estimated time of glacial retreat from various locations across the mainland and island archipelago. The majority of the landscape became mostly ice-free at lower elevations as recently as 15 ka (Lesnek et al., 2020). Minimum soil age for Spodosols formation of $<$ 300 yr has also been quantified through examination of recent glacial advances and retreat creating a chronosequence of glacial moraines (Alexander and Burt, 1996; Burt and Alexander, 1996; Chandler, 1943; Crocker and Dickson, 1957).

The formation of well-developed Spodosols requires a considerable amount of time, usually $>$ 1 ky for temperate regions on acidic parent materials (Sauer et al., 2008), a stable landscape in terms of erosional processes (Portes et al., 2018), and intense leaching conditions (Alexander et al., 1994; Mokma and Buurman, 1987; Sanborn et al., 2011). Our recent data (Portes et al., in preparation) on erosion rates using $^{239+240}$Pu and ^{13}C isotopes demonstrated that these soils are formed on stable slopes, with erosion/accumulation rates approaching zero on a decadal time scale. Therefore, although the studied soils have not been dated, they share similar forest cover density, tree height, understory cover, and morphological properties, indicating similar degree of soil development.

The minimum age estimate for a Spodosol in southeast Alaska was identified in a 250 yr old moraine (Alexander and Burt, 1996; Chandler, 1943). This 250 yr Spodosol was much less developed compared to the soils in this study where the soils are deeper, have much better developed spodic horizons in terms of color, structure, and thickness, and at least one order of magnitude higher pedogenic Fe concentrations. The soils of the current study are also more developed than a 550 yr Spodosol formed in an analogous environment on Vancouver Island, British Columbia, Canada (Singleton and Lavkulich, 1987) with at least one order of magnitude higher pedogenic Fe and at least twice the concentration of SOC in the spodic horizons. In southeast Alaska, the formation of mature Spodosols, in equilibrium with the environment, requires at least 500 yr and most likely 1kyr or more (Chandler, 1943). Therefore, the strong degree of soil development combined with a stable landscape

position suggests the studied soils are in equilibrium with current environmental conditions, likely older than 1 kyr, but younger than 10 ky when the post-glacial landscape stabilized.

Another line of evidence for the maturity of the regional Spodosols is the presence of Andic properties as about one-third of Spodosols in non-volcanic materials in the region meet the andic or aquandic subgroup requirements (Alexander et al., 1993). Andic properties in non-volcanic parent materials are considered evidence of steady-state conditions in the region because of rapid leaching and elevated SOC under a cool and wet climate. Although we did not measure P-retention, the other requirements for andic properties (i.e., $Al_o+^{1/2}Fe_o$, and bulk density) were easily met. The very low bulk density values for these soils are due to high SOC concentrations and abundant rock fragments, which is in line with other Spodosols with andic properties in the region (Alexander et al., 1993; D'Amore et al., 2011).

All of the evidence in the studied soils supports the conclusion that the soils are mature and well-developed Spodosols, likely older than 1 kyr, that appear to be fairly stable except for some occasional surface (20–30 cm deep) disturbance from windthrow (Bormann et al., 1995; Kramer et al., 2004).

5. Conclusions

The investigated soils represent the steady-state pedogenic conditions for upland soils in Northeast Pacific coastal temperate rainforests of North America. Podzolization homogenized soil formation across all lithologies, but the intensity of weathering and abundance of Fe oxides were controlled by the mineralogical composition of rock types. The high Fe concentration in all lithologies retard podzolization processes and would inhibit the genesis of Spodosols in most other temperate environments. Thus, well-developed, fine-textured, Fe-rich Spodosols are likely endemic to these coastal temperate rainforests. Our study demonstrates how podzolization in a coastal temperate rainforest drives pedological convergence from different rock types while preserving certain geochemical and mineralogical characteristics inherited from the parent materials. Therefore, future pedological studies should consider how differences in geochemical and mineralogical properties influence soil organic carbon dynamics, nutrient cycling, and forest productivity.

Declaration of Competing Interest

The authors declare that they have no known competing financial interests or personal relationships that could have appeared to influence the work reported in this paper.

Data availability

Data will be made available on request.

Acknowledgements

A portion of this research was performed on project award no. 51650 from the Environmental Molecular Sciences Laboratory, a DOE Office of Science User Facility sponsored by the Biological and Environmental Research program under Contract No. DE-AC05-76RL01830. We thank Randy Hesser (PNWRS) and Benjamin Pierce (University of Wisconsin River Falls) for the fieldwork assistance. We also thank Pauline Plumb (PNWRS), Mark Lukey (PNWRS), Emily Whitney (University of Alaska Southeast), Ken Severin (UAF), Don Butler (UAF) for the lab and logistical support. We also thank Prof. Elizabeth Solleiro-Rebolledo and Jaime Diaz Ortega (National Autonomous University of Mexico) for producing the thin sections. We also would like to thank the two reviewers and associate editor for the critical and insightful review of this manuscript.

Appendix A. Supplementary data

Supplementary data to this article can be found online at https://doi.org/10.1016/j.geoderma.2022.116211.

References

Alaback, P., Pojar, J., 1997. Vegetation from Ridgetop to Seashore. In: Schoonmaker, P. K., von Hagen, B., Wolf, W.C. (Eds.), The Rain Forests of Home: Profile of a North American Bioregion. Island Press, Washington, D.C., pp. 69–87

Alexander, E.B., Burt, R., 1996. Soil development on moraines of Mendenhall Glacier, southeast Alaska. 1. The moraines and soil morphology. Geoderma 72, 1–17. https://doi.org/10.1016/0016-7061(96)00021-3.

Alexander, E.B., Shoji, S., West, R., 1993. Andic soil properties of Spodosols in nonvolcanic materials of Southeast Alaska. Soil Sci. Soc. Am. J. 57 (2), 472–475.

Alexander, E.B., Ping, C.L., Krosse, P., 1994. Podzolization in ultramafic materials in Southeast Alaska. Soil Sci. 157 (1), 46–52.

Bain, D.C., 1977. The weathering of ferruginous chlorite in a podzol from Argyllshire, Scotland. Geoderma 17 (3), 193–208.

Bain, D.C., Mellor, A., Wilson, M.J., 1990. Nature and origin of an aluminous vermiculitic weathering product in acid soils from upland catchments in Scotland. Clay Miner. 25, 467–475. https://doi.org/10.1180/claymin.1990.025.4.05.

Balland, C., Poszwa, A., Leyval, C., Mustin, C., 2010. Dissolution rates of phyllosilicates as a function of bacterial metabolic diversity. Geochim. Cosmochim. Acta 74, 5478–5493. https://doi.org/10.1016/j.gca.2010.06.022.

Barnhisel, R.I., Bertsch, P.M., 1989. Chlorites and Hydroxy-Interlayered Vermiculite and Smectite. In: Minerals in Soil Environments. Soil Science Society of America, Madison, WI, pp. 729–788.

Barrett, L.R., Schaetzl, R.J., 1992. An examination of podzolization near Lake Michigan using chronofunctions. Can. J. Soil Sci. 72 (4), 527–541.

Birkeland, P.W., 1984. Soils and Geomorphology, second. ed. Oxford University, New York.

Bormann, B.T., Spaltenstein, H., McClellan, M.H., Ugolini, F.C., Jr., K.C., Nay, S.M., 1995. Rapid soil development after windthrow disturbance in pristine forests. J. Ecol. 83 (5), 747.

Brimhall, G.H., Christopher J., L., Ford, C., Bratt, J., Taylor, G., Warin, O., 1991. Quantitative geochemical approach to pedogenesis: importance of parent material reduction, volumetric expansion, and eolian influx in lateritization. Geoderma 51 (1-4), 51–91.

Brock, T., West, R., Paustian, Steven, J., 1996. A landform classification guide for the Alaska Region.

Bulmer, C.E., Lavkulich, L.M., 1994. Pedogenic and geochemical processes of ultramafic soils along a climatic gradient in southwestern British Columbia. Can. J. Soil Sci. 74 (2), 165–177.

Burt, R., Alexander, E.B., 1996. Soil development on moraines of Mendenhall Glacier, southeast Alaska. 2. Chemical transformations and soil micromorphology. Geoderma 72, 19–36. https://doi.org/10.1016/0016-7061(96)00022-5.

Buurman, P., Jongmans, A.G., 2005. Podzolisation and soil organic matter dynamics. Geoderma 125, 71–83. https://doi.org/10.1016/j.geoderma.2004.07.006.

Carrara, P.E., Ager, T.A., Baichtal, J.F., 2007. Possible refugia in the Alexander Archipelago of southeastern Alaska during the late Wisconsin glaciation. Can. J. Earth Sci. 44 (2), 229–244.

National Climatic Data Center, 2020. Alaska climate normals 1971-2000 [WWW Document].

Chadwick, O.A., Brimhall, G.H., Hendricks, D.M., 1990. From a black to a gray box - a mass balance interpretation of pedogenesis. Geomorphology 3, 369–390. https://doi.org/10.1016/0169-555X(90)90012-F.

Chandler, R.F., 1943. The time required for podzol profile formation as evidenced by the mendenhall glacial deposits Near Juneau, Alaska. Soil Sci. Soc. Am. J. 7 (C), 454–459.

Chapman, S.L., Horn, M.E., 1968. Parent material uniformity and origin of silty soils in northwest arkansas based on zirconium-titanium contents. Soil Sci. Soc. Am. 32 (2), 265–271.

Chen, P.-Y., 1977. Table of key lines in X-ray powder diffraction patterns of minerals in clays and associated rocks: Indiana Geological Survey Occasional Paper.

Cornu, S., Lucas, Y., Lebon, E., Ambrosi, J.P., Luizão, F., Rouiller, J., Bonnay, M., Neal, C., 1999. Evidence of titanium mobility in soil profiles, Manaus, central Amazonia. Geoderma 91, 281–295. https://doi.org/10.1016/S0016-7061(99)00007-5.

Courchesne, F., Turmel, M.-C., Beauchemin, P., 1996. Magnesium and potassium release by weathering in spodosols: grain surface coating effects. Soil Sci. Soc. Am. J. 60, 1188–1196. https://doi.org/10.2136/sssaj1996.03615995006000040033x.

Cremeens, D.L., Mokma, D.L., 1986. Argillic horizon expression and classification in the soils of two Michigan hydrosequences. Soil Sci. Soc. Am. J. 50 (4), 1002–1007.

Crocker, R.L., Dickson, B.A., 1957. Soil Development on the Recessional Moraines of the Herbert and Mendenhall Glaciers, South-Eastern Alaska. J. Ecol. 45, 169. https://doi.org/10.2307/2257083.

Dahms, D., Favilli, F., Krebs, R., Egli, M., 2012. Soil weathering and accumulation rates of oxalate-extractable phases derived from alpine chronosequences of up to 1Ma in age. Geomorphology 151–152 (May), 99–113. https://doi.org/10.1016/j.geomorph.2012.01.021.

D'Amore, D.V., Bonzey, N.S., Berkowitz, J., Rüegg, J., Bridgham, S., 2011. Holocene soil-geomorphic surfaces influence the role of salmon-derived nutrients in the coastal

temperate rainforest of Southeast Alaska. Geomorphology 126, 377–386. https://doi.org/10.1016/j.geomorph.2010.04.014.
D'Amore, D.V., Ping, C.L., Herendeen, P.A., 2015. Hydromorphic soil development in the coastal temperate rainforest of Alaska. Soil Sci. Soc. Am. J. 79, 698–709. https://doi.org/10.2136/sssaj2014.08.0322.
D'Amore, D.V., Fellman, J.B., Edwards, R.T., Hood, E., Ping, C.-L., 2012. Hydropedology of the North American Coastal Temperate Rainforest. In: Hydropedology. Elsevier, pp. 351–380.
Dorn, R.I., 1983. Cation-ratio dating: A new rock varnish age-determination technique. Quaternary Res. 20 (1), 49–73. https://doi.org/10.1016/0033-5894(83)90065-0.
Duchaufour, P.h., Souchier, B., 1978. Roles of iron and clay in Genesis of acid soils under a humid, temperate climate. Geoderma 20, 15–26. https://doi.org/10.1016/0016-7061(78)90046-0.
Egli, M., Fitze, P., 2000. Formulation of pedologic mass balance baed on immobile elements: a revision. Soil Sci. 165, 437–443.
Egli, M., Mirabella, A., Fitze, P., 2001. Clay mineral formation in soils of two different chronosequences in the Swiss Alps. Geoderma 104, 145–175. https://doi.org/10.1016/S0016-7061(01)00079-9.
Egli, M., Mirabella, A., Sartori, G., Fitze, P., 2003. Weathering rates as a function of climate: Results from a climosequence of the Val Genova (Trentino, Italian Alps). Geoderma 111, 99–121. https://doi.org/10.1016/S0016-7061(02)00256-2.
Egli, M., Mirabella, A., Mancabelli, A., Sartori, G., 2004. Weathering of soils in Alpine areas as influenced by climate and parent material. Clays Clay Miner. 52, 287–303. https://doi.org/10.1346/CCMN.2004.0520304.
Ferro-Vázquez, C., Nóvoa-Muñoz, J.C., Costa-Casais, M., Klaminder, J., Martínez-Cortizas, A., 2014. Metal and organic matter immobilization in temperate podzols: A high resolution study. Geoderma 217–218, 225–234. https://doi.org/10.1016/j.geoderma.2013.10.006.
Ferro-Vázquez, C., Nóvoa-Muñoz, J.C., Klaminder, J., Gómez-Armesto, A., Martínez-Cortizas, A., 2020. Comparing podzolization under different bioclimatic conditions. Geoderma 377, 114581. https://doi.org/10.1016/j.geoderma.2020.114581.
FS-R10-TNF, 2016. Landtype Associations of the Tongass National Forest, R10-TP-161st ed. U.S. Forest Service, Alaska Region.
Gehrels, G.E., Berg, H.C., 1992. Geologic map of southeastern Alaska: U.S. Geological Survey Miscellaneous Investigations Series Map 1867, 1 sheet, scale 1:600,000.
Gehrels, G.E., Berg, H.C., 1994. Geology of southeastern Alaska. In: Plafker, G., Berg, H. C. (Eds.), The Geology of North America. Geological Society of America, Boulder, Colorado, pp. 451–467.
Gillot, F., Righi, D., Elsass, F., 2000. Pedogenic smectites in podzols from central Finland: An analytical electron microscopy study. Clays Clay Miner. 48, 655–664. https://doi.org/10.1346/CCMN.2000.0480607.
Harrington, C.D., Whitney, J.W., 1987. Scanning electron microscope method for rock-varnish dating. Geology 15 (10), 967–970. https://doi.org/10.1130/0091-7613(1987)15<967:SEMMFR>2.0.CO;2.
Heilman, P.E., Gass, C.R., 1974. Parent materials and chemical properties of mineral soils in southeast Alaska. Soil Sci. 117 (1), 21–27.
Heusser, C.J., 1960. Late-Pleistocene environments of north Pacific North America. Am. Geogr. Soc. Spec. Publ 35, 308.
Hunt, A.G., Egli, M., Faybishenko, B., 2021. Hydrogeology, chemical weathering, and soil formation, 1st ed. John Wiley and Sons, American Geophysical Union, Hoboken, NJ.
Inskeep, W.P., Clayton, J.L., Mogk, D.W., 1993. Naturally weathered plagioclase grains from the Idaho batholith: observations using scanning electron microscopy. Soil Sci. Soc. Am. J. 57, 851–860. https://doi.org/10.2136/sssaj1993.03615995005700030036x.
Jansen, B., Nierop, K.G.J., Verstraten, J.M., 2003. Mobility of Fe(II), Fe(III) and Al in acidic forest soils mediated by dissolved organic matter: Influence of solution pH and metal/organic carbon ratios. Geoderma 113, 323–340. https://doi.org/10.1016/S0016-7061(02)00368-3.
Jochum, K.P., Nohl, U., Herwig, K., Lammel, E., Stoll, B., Hofmann, A.W., 2005. GeoReM: A new geochemical database for reference materials and isotopic standards. Geostand. Geoanal. Res. 29, 333–338. https://doi.org/10.1111/j.1751-908X.2005.tb00904.x.
Kaiser, K., Eusterhues, K., Rumpel, C., Guggenberger, G., Kögel-Knabner, I., 2002. Stabilization of organic matter by soil minerals - Investigations of density and particle-size fractions from two acid forest soils. J. Plant Nutr. Soil Sci. 165, 451–459. https://doi.org/10.1002/1522-2624(200208)165:4<451::AID-JPLN451>3.0.CO;2-B.
Kindler, R., Siemens, J., Kaiser, K., Walmsley, D.C., Bernhofer, C., Buchmann, N., Cellier, P., Eugster, W., Gleixner, G., Grunwald, T., Heim, A., Ibrom, A., Jones, S.K., Jones, M., Klumpp, K., Kutsch, W., Larsen, K.S., Lehuger, S., Loubet, B., Mckenzie, R., Moors, E., Osborne, B., Pilegaard, K., Rebmann, C., Saunders, M., Schmidt, M.W.I., Schrumpf, M., Seyfferth, J., Skiba, U., Soussana, J.F., Sutton, M.A., Tefs, C., Vowinckel, B., Zeeman, M.J., Kaupenjohann, M., 2011. Dissolved carbon leaching from soil is a crucial component of the net ecosystem carbon balance. Glob. Change Biol. 17, 1167–1185. https://doi.org/10.1111/j.1365-2486.2010.02282.x.
Kitagawa, Y., 2005. Characteristics of clay minerals in podzols and podzolic soils. Soil Sci. Plant Nutr. 51, 151–158. https://doi.org/10.1111/j.1747-0765.2005.tb00020.x.
Kleber, M., Bourg, I.C., Coward, E.K., Hansel, C.M., Myneni, S.C.B., Nunan, N., 2021. Dynamic interactions at the mineral–organic matter interface. Nat. Rev. Earth Environ. 2, 402–421. https://doi.org/10.1038/s43017-021-00162-y.
Kögel-Knabner, I., Amelung, W., 2021. Soil organic matter in major pedogenic soil groups. Geoderma 384, 114785.
Kögel-Knabner, I., Guggenberger, G., Kleber, M., Kandeler, E., Kalbitz, K., Scheu, S., Eusterhues, K., Leinweber, P., 2008. Organo-mineral associations in temperate soils: Integrating biology, mineralogy, and organic matter chemistry. J. Plant Nutr. Soil Sci. 171, 61–82. https://doi.org/10.1002/jpln.200700048.
Kramer, M.G., Chadwick, O.A., 2018. Climate-driven thresholds in reactive mineral retention of soil carbon at the global scale. Nat. Clim. Change 8, 1104–1108. https://doi.org/10.1038/s41558-018-0341-4.
Kramer, M.G., Sollins, P., Sletten, R.S., 2004. Soil carbon dynamics across a windthrow disturbance sequence in southeast Alaska. Ecology 85, 2230–2244. https://doi.org/10.1890/02-4098.
Lesnek, A.J., Briner, J.P., Lindqvist, C., Baichtal, J.F., Heaton, T.H., 2018. Deglaciation of the pacific coastal corridor directly preceded the human colonization of the Americas. Sci. Adv. 4, 1–8. https://doi.org/10.1126/sciadv.aar5040.
Lesnek, A.J., Briner, J.P., Baichtal, J.F., Lyles, A.S., 2020. New constraints on the last deglaciation of the Cordilleran Ice Sheet in coastal Southeast Alaska. Quat. Res. 96, 140–160.
Lichter, J., 1998. Rates of weathering and chemical depletion in soils across a chronosequence of Lake Michigan sand dunes. Geoderma 85 (4), 255–282. https://doi.org/10.1016/S0016-7061(98)00026-3.
Lundström, U.S., 1993. The role of organic acids in the soil solution chemistry of a podzolized soil. J. Soil Sci. 44, 121–133. https://doi.org/10.1111/j.1365-2389.1993.tb00439.x.
Lundström, U.S., Van Breemen, N., Bain, D., 2000. The podzolization process. A review. Geoderma 94, 91–107. https://doi.org/10.1016/S0016-7061(99)00036-1.
Lützow, M.V., Kögel-Knabner, I., Ekschmitt, K., Matzner, E., Guggenberger, G., Marschner, B., Flessa, H., 2006. Stabilization of organic matter in temperate soils: Mechanisms and their relevance under different soil conditions - A review. Eur. J. Soil Sci. 57, 426–445. https://doi.org/10.1111/j.1365-2389.2006.00809.x.
McClelland, W.C., Gehrels, G.E., Samson, S.D., Patchett, P.J., 1992. Protolith relations of the Gravina Belt and Yukon-Tanana Terrane in Central Southeastern Alaska. J. Geol. 100 (1), 107–123.
McKeague, J.A., Day, J.H., 1966. Dithionite and oxalate extractable Fe and Al as aids in differentiating various classes of soils. Can. J. Soil Sci. 46, 13–22. https://doi.org/10.4141/cjss66-003.
McKeague, J.A., Brydon, J.E., Miles, N.M., 1971. Differentiation of forms of extractable iron and aluminum in soils. Soil Sci. Am. J. 35, 33–38. https://doi.org/10.2136/sssaj1971.03615995003500010016x.
McKeague, J.A., DeConinck, F., Franzmeier, D.P., 1983. Chapter 6 spodosols. Dev. Soil Sci. 11, 217–252. https://doi.org/10.1016/S0166-2481(08)70617-2.
McNicol, G., Bulmer, C., D'Amore, D., Sanborn, P., Saunders, S., Giesbrecht, I., Arriola, S. G., Bidlack, A., Butman, D., Buma, B., 2019. Large, climate-sensitive soil carbon stocks mapped with pedology-informed machine learning in the North Pacific coastal temperate rainforest. Environ. Res. Lett. 14 (1), 014004.
Mehra, O.P., 1958. Iron oxide removal from soils and clays by a dithionite-citrate system buffered with sodium bicarbonate. Clays Clay Miner. 7, 317–327. https://doi.org/10.1346/ccmn.1958.0070122.
Meunier, A., 2007. Soil hydroxy-interlayered minerals: A re-interpretation of their crystallochemical properties. Clays Clay Miner. 55, 380–388. https://doi.org/10.1346/CCMN.2007.0550406.
Mikutta, R., Kleber, M., Jahn, R., 2005. Poorly crystalline minerals protect organic carbon in clay subfractions from acid subsoil horizons. Geoderma 128, 106–115. https://doi.org/10.1016/j.geoderma.2004.12.018.
Miller, R.D., 1975. Surficial geologic map of the Juneau urban area and vicinity, Alaska: U.S. Geological Survey Miscellaneous Investigations Series Map 885, 1 sheet, scale 1: 48,000.
Mirabella, A., Egli, M., Carnicelli, S., Sartori, G., 2002. Influence of parent material on clay minerals formation in Podzols of Trentino, Italy. Clay Miner. 37, 699–707. https://doi.org/10.1180/0009855023740071.
Mokma, D.L., Buurman, P., 1987. Podzols and podzolization in temperate regions. Soil Sci. 144 (1), 79.
Mokma, D.L., Yli-Halla, M., Lindqvist, K., 2004. Podzol formation in sandy soils of Finland. Geoderma 120 (3-4), 259–272.
Musielok, Ł., Drewnik, M., Szymański, W., Stolarczyk, M., Gus-Stolarczyk, M., Skiba, M., 2021. Conditions favoring local podzolization in soils developed from flysch regolith – A case study from the Bieszczady Mountains in southeastern Poland. Geoderma 381, 114667.
Nelson, L.-A., Sanborn, P., Cade-Menun, B.J., Walker, I.J., Lian, O.B., 2021. Pedological trends and implications for forest productivity in a Holocene soil chronosequence, Calvert Island, British Columbia, Canada. Can. J. Soil Sci. 19 (June), 1–19. https://doi.org/10.1139/cjss-2021-0033.
Nesbitt, H.W., Young, G.M., 1982. Early proterozoic climates and plate motions inferred from major element chemistry of lutites. Nature 299 (5885), 715–717.
Nierop, K.G.J., Jansen, B., Verstraten, J.M., 2002. Dissolved organic matter, aluminium and iron interactions: precipitation induced by metal/carbon ratio, pH and competition. Sci. Total Environ. 300, 201–211. https://doi.org/10.1016/S0048-9697(02)00254-1.
Pansu, M., Jacques, G., 2006. Handbook of Soil Analysis Mineralogical, Organic and Inorganic Methods. Springer Verlag, Berlin Heildelberg.
Parfitt, R.L., Kimble, J.M., 1989. Conditions for formation of allophane in soils. Soil Sci. Soc. Am. J. 53, 971–977. https://doi.org/10.2136/sssaj1989.03615995005300030057x.
Ping, C.L., Clark, M.H., D'Amore, D., Michaelson, G.J., Swanson, D.K., 2017. Soils of Alaska: LRRs W1, W2, X1, X2, and Y, in: West, L.T., Singer, M.J., Hartemink, A.E. (Eds.), The Soils of the USA. Cham, pp. 329–350.
Portes, R., Dahms, D., Brandová, D., Raab, G., Christl, M., Kühn, P., Ketterer, M., Egli, M., 2018. Evolution of soil erosion rates in alpine soils of the Central Rocky Mountains using fallout Pu and δ13C. Earth Planet. Sci. Lett. 496, 257–269. https://doi.org/10.1016/j.epsl.2018.06.002.

Portes, R.C., Spinola, D.N., Santiago, J., Carlos, J., Marciano, L., Inácio, E., Filho, F., Kühn, P., Ernesto, C., Reynaud, G., Port, P., 2016. Pedogenesis across a climatic gradient in tropical high mountains, Cordillera Blanca — Peruvian Andes. Catena 147, 441–452. https://doi.org/10.1016/j.catena.2016.07.027.

Protz, R., Martini, I.P., Ross, G.J., Terasmae, J., 1984. Rate of Podzolic soil formation near Hudson Bay, Ontario. Can. J. Soil Sci. 64 (1), 31–49.

Protz, R., Shipitalo, M.J., Ross, G.J., Terasmae, J., 1988. Podzolic soil development in the southern James Bay lowlands, Ontario. Can. J. Soil Sci. 68 (2), 287–305.

Rasmussen, C., Throckmorton, H., Liles, G., Heckman, K., Meding, S., Horwath, W., 2018. Controls on soil organic carbon partitioning and stabilization in the California Sierra Nevada. Soil Syst. 2, 41. https://doi.org/10.3390/soilsystems2030041.

Righi, D., Petit, S., Bouchet, A., 1993. Characterization of hydroxy-interlayered vermiculite and illite/smectite interstratified minerals from the weathering of chlorite in a cryorthod. Clays Clay Miner. 41, 484–495. https://doi.org/10.1346/CCMN.1993.0410409.

Sanborn, P., Lamontagne, L., Hendershot, W., 2011. Podzolic soils of Canada: Genesis, distribution, and classification. Can. J. Soil Sci. 91, 843–880. https://doi.org/10.4141/cjss10024.

Sanborn, P., Lavkulich, L.M., 1989. Ferro-humic podzols of coastal British Columbia: II. Micromorphology and genesis. Soil Sci. Soc. Am. J. 53, 517–526. https://doi.org/10.2136/sssaj1989.03615995005300020036x.

Sauer, D., Sponagel, H., Sommer, M., Giani, L., Jahn, R., Stahr, K., 2007. Podzol: Soil of the year 2007. A review on its genesis, occurrence, and functions. J. Plant Nutr. Soil Sci. 170, 581–597. https://doi.org/10.1002/jpln.200700135.

Sauer, D., Schülli-Maurer, I., Sperstad, R., Sørensen, R., Stahr, K., 2008. Podzol development with time in sandy beach deposits in southern Norway. J. Plant Nutr. Soil Sci. 171, 483–497. https://doi.org/10.1002/jpln.200700023.

Schaetzl, R.J., 1998. Lithologic discontinuities in some soils on drumlins: theory, detection, and application. Soil Sci. 163 (7), 570–590.

Schoeneberger, P.J., Wysocki, D.A., Benham, E.C., 2012. Field book for describing and sampling soils, Version 3.0. Lincoln, NE.

Schwertmann, U., 1964. The differentiation of iron oxides in soil by extraction with ammonium oxalate solution. Z. Pflanzenernaehr. Bodenkd 105, 194–202.

Schwertmann, U., Kodama, H., Fischer, W.R., 1986. Mutual interactions between organics and iron oxides. Soil Science Society of America.

Schwertmann, U., Taylor, R.M., 1989. Iron oxides. In: Dixon, J.B., Weed, S.B. (Eds.), Minerals in Soil Environments. Soil Science Society of America, Madison, Wisconsin, pp. 379–438.

Shoji, S., Nanzyo, M., Dahlgren, R.A., 1993. Volcanic ash soils - Genesis, properties and utilization, Statewide Agricultural Land Use Baseline 2015. Elsevier Science, Amsterdam.

Singleton, G.A., Lavkulich, L.M., 1987. A soil chronosequence on beach sands, Vancouver Island, British Columbia. Can. J. Soil Sci. 67 (4), 795–810.

Skiba, M., 2001. The origin of kaolinite from the Tatra Mts. Podzols. Mineral. Polonica 32, 67–76.

Skiba, M., 2007. Clay mineral formation during podzolization in an Alpine environment of the Tatra Mountains, Poland. Clays Clay Miner. 55, 618–634. https://doi.org/10.1346/CCMN.2007.0550609.

Slessarev, E.W., Chadwick, O.A., Sokol, N.W., Nuccio, E.E., Pett-Ridge, J., 2022. Rock weathering controls the potential for soil carbon storage at a continental scale. Biogeochemistry 157, 1–13. https://doi.org/10.1007/s10533-021-00859-8.

Soil Survey Staff, 2014. Keys to soil taxonomy. Soil Conservation Service 12, 360.

Soil Survey Staff, 2022. Web Soil Survey [WWW Document]. ULLOA Series. URL https://soilseries.sc.egov.usda.gov/OSD_Docs/U/ULLOA.html.

Sommer, M., Halm, D., Weller, U., Zarei, M., Stahr, K., 2000. Lateral podzolization in a granite landscape. Soil Sci. Soc. Am. J. 64, 1434–1442. https://doi.org/10.2136/sssaj2000.6462069x.

Soil Survey Staff, 2014b. Soil Survey Field and Laboratory Methods Manual. United States Department of Agriculture, Natural Resources Conservation Service 487. https://doi.org/10.13140/RG.2.1.3803.8889.

Stiles, C.A., Mora, C.I., Driese, S.G., 2001. Pedogenic iron-manganese nodules in Vertisols: A new proxy for paleoprecipitation? Geology 29, 943–946. https://doi.org/10.1130/0091-7613(2001)029<0943:PIMNIV>2.0.CO;2.

Stumm, W., Morgan, J.J., 1996. Aquatic chemistry: chemical equilibria and rates in natural waters. Wiley, New York.

Sudom, M.D., J., Star, 1971. Use of Quartz, Zirconium and Titanium As Indices in Pedological Studies. Canadian Journal of Soil Science 51, 385–396. https://doi.org/10.4141/cjss71-052.

Ugolini, F.C., 1966. Soils. Institute of Polar Studies Report, 20. Soil development and ecological succession in a deglaciated area of Muir inlet, southeast Alaska. Columbus, OH.

van Breemen, N., Buurman, P., 2003. Soil Formation, 2nd ed. Kluwer Academic Publishers, New York.

Vasyukova, E.V., Oliva, P., Viers, J., Martin, F., Dupré, B., Pokrovsky, O.S., 2019. Chemical weathering of mafic rocks in boreal subarctic environment (northwest Russia) under influence of glacial moraine deposits. Chem. Geol. 509, 115–133. https://doi.org/10.1016/j.chemgeo.2018.12.033.

Velbel, M.A., 1989. Weathering of hornblende to ferruginous products by a dissolution-reprecipitation mechanism. Petrography and stoichiometry. Clays Clay Miner. 37, 515–524. https://doi.org/10.1346/CCMN.1989.0370603.

Velde, B., Meunier, A., 2008. The Origin of Clay Minerals in Soil and Weathered Rocks. Springer-Verlag, Berlin Heildelberg.

Von Lützow, M., Kögel-Knabner, I., Ludwig, B., Matzner, E., Flessa, H., Ekschmitt, K., Guggenberger, G., Marschner, B., Kalbitz, K., 2008. Stabilization mechanisms of organic matter in four temperate soils: Development and application of a conceptual model. J. Plant Nutr. Soil Sci. 171, 111–124. https://doi.org/10.1002/jpln.200700047.

Wada, K., 1977. Allophane and imogolite, in: Dixon, J.B., Weed, S.B. (Eds.), Minerals in Soil Environments. Soil Science Society of America, p. 1087.

Waroszewski, J., Egli, M., Kabala, C., Kierczak, J., Brandova, D., 2016. Mass fluxes and clay mineral formation in soils developed on slope deposits of the Kowarski Grzbiet (Karkonosze Mountains, Czech Republic/Poland). Geoderma 264, 363–378. https://doi.org/10.1016/j.geoderma.2015.08.044.

Whalen, M.T., Śliwiński, M.G., Payne, J.H., Day, J.E., Chen, D., Da Silva, A.C., 2015. Chemostratigraphy and magnetic susceptibility of the Late Devonian Frasnian-Famennian transition in western Canada and southern China: Implications for carbon and nutrient cycling and mass extinction. Geol. Soc. Spec. Pub. 414, 37–72. https://doi.org/10.1144/SP414.8.

Wilson, M.J., 1999. The origin and formation of clay minerals in soils: past, present and future perspectives. Clay Miner. 34, 7–25. https://doi.org/10.1180/000985599545957.

Wilson, M.J., 2004. Weathering of the primary rock-forming minerals: processes, products and rates. Clay Miner. 39, 233–266. https://doi.org/10.1180/0009855043930133.

Wolf, E.C., Mitchell, A.P., Schoonmaker, P.K., 1995. The rain forests of home: an atlas of people and place.

Yaalon, D.H. (Ed.), 1971. Criteria for the recognition and classification of paleosols, in: Paleopedology: Origin, Nature and Dating of Paleosols. Israel Universities Press, Jerusalem, pp. 153–158.